Use of Unoccupied Aerial Systems (UAS) to Evaluate Salt Marsh Condition and Vulnerability to Sea Level Rise

November 13, 2023

Scott Jackson, Ryan Wicks, Joshua Ward, Kate Fickas, Eva Gerstle, Ayushi Shrivastava, Stephen Fickas, and Charles Schweik

University of Massachusetts Amherst

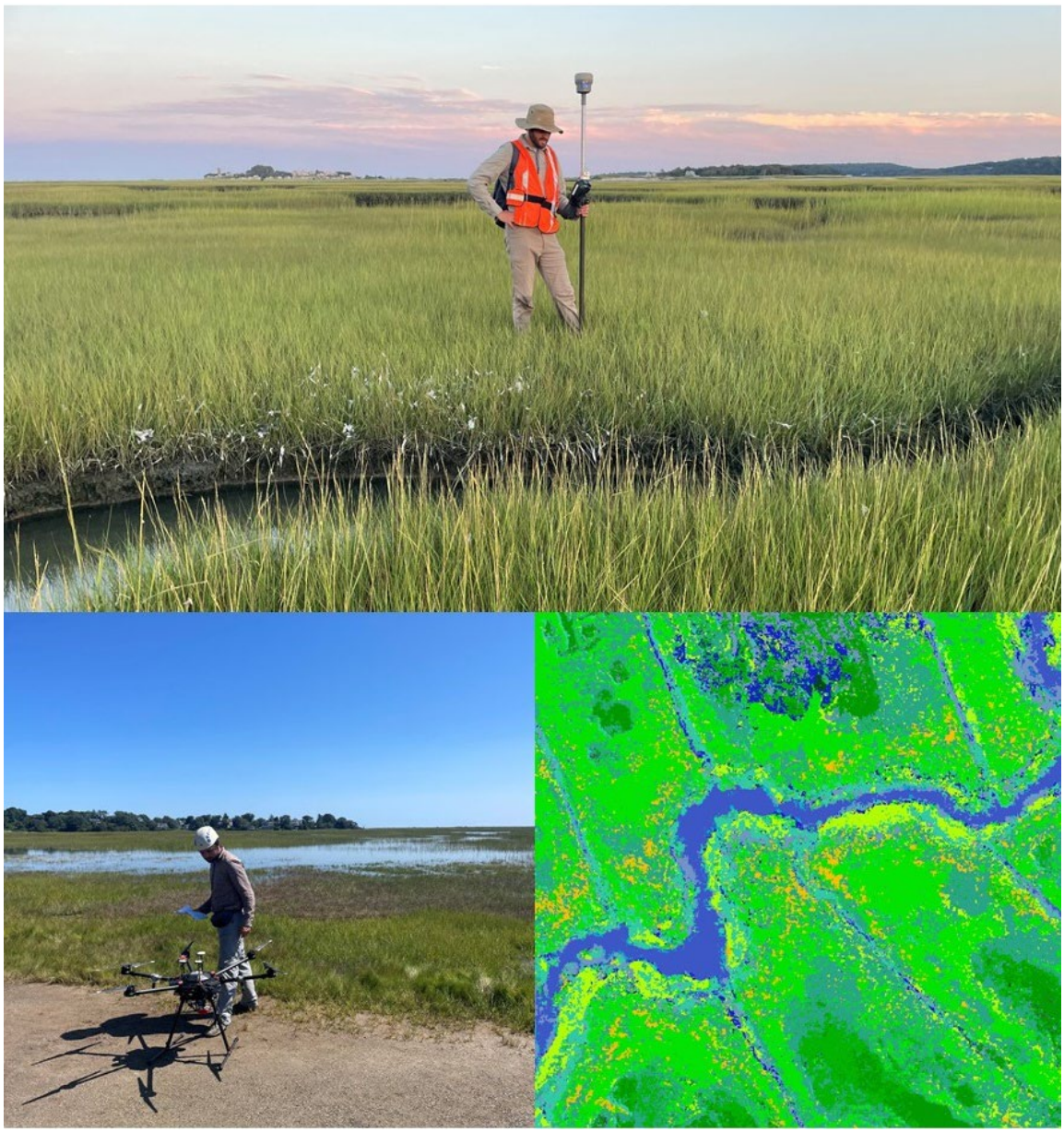

Progress Report for EPA FY 2019-2020 (CD 00A00291-3) and FY 2021-2022 (CD 00A00790-1) Wetlands Program Development Grants

Contents

List of Tables

List of Figures

List of Abbreviations

CAPS	Conservation Assessment and Prioritization System
CHM	Canopy Height Models
CSF	Cloth Simulation Filtering
DEM	Digital Elevation Model
DTM	Digital Terrain Model
GCP	Ground Control Points
GNSS	Global Navigation Satellite System
ICS	Iterative Classification Scheme
IEI	Index of Ecological Integrity
LiDAR	Light Detection and Ranging
MaCORS	Massachusetts Continuously Operating Reference Station Network
NIR	Near Infrared
PPK	Post-Processed Kinematic
QAPP	Quality Assurance Project Plan
QA/QC	Quality Assurance/Quality Control
RESEPI	Remote Sensing Payload Instrument
RFM	Random Forest Modeling
RGB	Red, Green, Blue
RINEX	Receiver Independent Exchange Format
RMSE	Root Mean Square Error
RTK	Real-Time Kinematic
SWIR	Short-wave Infrared
UAS	Unoccupied Aerial Systems
UAV	Unoccupied Aerial Vehicle

Acknowledgements

We appreciate the towns, landowners, and land conservation organizations who have supported this project by providing permits, access to field sites, facilities, and personnel. It has been a pleasure to work with The Trustees of Reservations, Massachusetts Audubon Society, Harwich Conservation Trust, Chatham Conservation Commission, MA Coastal Zone Management (CZM), Town of Scituate, Scituate Country Club, Town of Barnstable, Sandy Neck Beach Park, Massachusetts Department of Conservation and Recreation (DCR), Marine Biological Laboratory, and Woods Hole Research Center. We acknowledge and thank the following people who materially contributed to this project: Marc Carullo, Daniel Myers, Emily Lozier, Diana Holmes, Armand Martinez, Taylor Lo, Matthew Jusino, Zachary Fouser, Phoebe Gelbard, David Price, Georgia Stuart, Sophia Somerscales, and Devin Clark. Special thanks go to Amanda Davis, Helena Koszewski and Brett Barnard for sustained contributions to this project and to Chengbo Ai from the UMass Department of Civil and Environmental Engineering for lending us his LiDAR sensor.

The U.S. EPA provided the primary funding for this project, most recently via Wetland Program Development Grants CD 00A00291-3 and CD 00A00790-1. Additional funding came from the UMass Center for Agriculture, Food, and the Environment in the form of funding for a summer undergraduate intern for each of our six field seasons, the Doris Duke Foundation, which provided funding for two Conservation Scholar internships, in-kind contributions from Dr. Stephen Fickas' lab at the University of Oregon, and in-kind matching funds from the University of Massachusetts Amherst.

Use of Unoccupied Aerial Systems (UAS) to Evaluate Salt Marsh Condition and Vulnerability to Sea Level Rise

Introduction

The University of Massachusetts Amherst, Massachusetts Coastal Zone Management and Massachusetts Department of Environmental Protection have been collaborating in the development of methods for evaluating wetland condition since 2007. A central component of the Massachusetts Assessment and Monitoring Program is CAPS, the Conservation Assessment and Prioritization System, a Level 1, landscape-scale modeling approach for evaluating ecological integrity of the Commonwealth's lands, wetlands and waters. Over the years, we have expanded and improved the CAPS models, creating new metrics and using Level 3, intensive site assessments to test and validate CAPS ecological integrity models for streams, forested wetlands, shrub swamps and salt marshes.

Using biological field data from Level 3 assessments, we were able to create robust Indices of Biological Integrity (IBIs) that corresponded to Index of Ecological Integrity (IEI) gradients for streams and forested wetlands, but not salt marshes. We suspected that the poor performance of CAPS ecological integrity models for salt marshes resulted from a lack of metrics for important salt marsh stressors related to sediment dynamics, bank erosion, effects of increased nutrient loading on peat accretion, changes in marsh elevation relative to sea level rise, crab herbivory, and crab burrowing effects on peat density and stability. In 2018, we began investigating the potential for using Unoccupied Aerial Systems (UAS; drones and sensors) to assess salt marsh condition and vulnerability to sea level rise.

Fieldwork in salt marshes is challenging because ground access is difficult, due to water features within marshes and often-unstable substrate, and limited amount of time available to access the marsh and collect data before that access is cut off by high tides. Remote sensing data (satellite imagery and aerial photography) has potential for salt marsh assessment, but their usefulness is limited because those data are not always available for stages in the tide cycle when specific characteristics need to be assessed. UAS offers the opportunity to collect multispectral data at very high resolution during critical stages in the tide cycle (low, mid, high and spring tides).

The primary objective of our Salt Marsh UAS project has been to evaluate the potential of UAS for assessing salt marsh condition and vulnerability to sea level rise and other stressors. Ultimately, we hope to use UAS to collect data for assessing salt marsh condition and vulnerability, and then scale up the analysis using available satellite and/or aerial photogrammetry for comprehensive assessments of salt marshes statewide.

All work funded by EPA grants was conducted according to a Quality Assurance Project Plan (QAPP, RFA# 18095) and associated Standard Operating Procedures. Some complementary components of the project were funded by other sources. The work took place at nine salt marsh sites in Massachusetts (see Appendix A). Landowner permission was acquired for access to each of our study sites. Multi-spectral imaging data were acquired via UAS, including visible Red/Green/Blue (RGB), Red-Edge, Near Infrared (NIR), Short-wave Infrared (SWIR), and LiDAR. Multiple flights were flown for each site throughout the growing season in an effort to capture seasonal spectral information from the changing dynamics in salt marsh plant canopy as well as to capture spectral information of water in and around the salt marsh vegetation across various tidal stages. We also used ground-based data collection to

acquire information about salt marsh land cover (vegetation, bare ground, and water features) to train and validate classification models, and HOBO water loggers to characterize tidal hydrology.

This report describes various components of the research conducted since our previous report (Jackson et al., 2021, "2021 Report"), including:

- UAS data collection and processing
- Salt marsh classification mapping: data analysis and modeling
- Water logger arrays, specifically timed UAS flights, and inundation mapping
- Identification of embankments and assessment of impacts
- Identification and mapping of eroding creek banks
- Effects of ribbed mussels on salt marsh surface elevation

UAS Data Collection and Processing

The QAPP and our 2021 report provides information about UAS flight preparation and implementation, and data processing. In this section, we report a new configuration for one of our sites, collection of additional training and validation data, summaries of drone-based photogrammetry products, and the development of digital elevation, digital terrain, and canopy height models.

A New Configuration for the Barnstable Site

Our previous Barnstable site, on the southeast side of the Barnstable Great Marsh, was located 4.5 km from runway 15 at Hyannis Airport (KHYA). Due to the close proximity of the study site to the airport, standard aircraft operations proved to be a significant safety hazard for our UAS operations. In the spring of 2023, our team contacted the Town of Barnstable to inquire about establishing a new study site on the northeast side of the Barnstable Great Marsh, further from the airport. With permission from the town and Sandy Neck Beach Park, we plotted new site boundaries that took ecological interests and airport operations into account (Figure 1).

The new Barnstable Great Marsh study site, hereafter referred to as “Barnstable”, is located in the northwest portion of the Barnstable Great Marsh in the town of Barnstable, and is managed as part of the Sandy Neck Beach Park. The boundaries of the study site were chosen to include both ditched and un-ditched areas. We installed nine ground control points (GCPs) throughout the site. The flight footprint covers 40.5 hectares (100 acres) and has a perimeter of 2.91 km (1.8 miles).

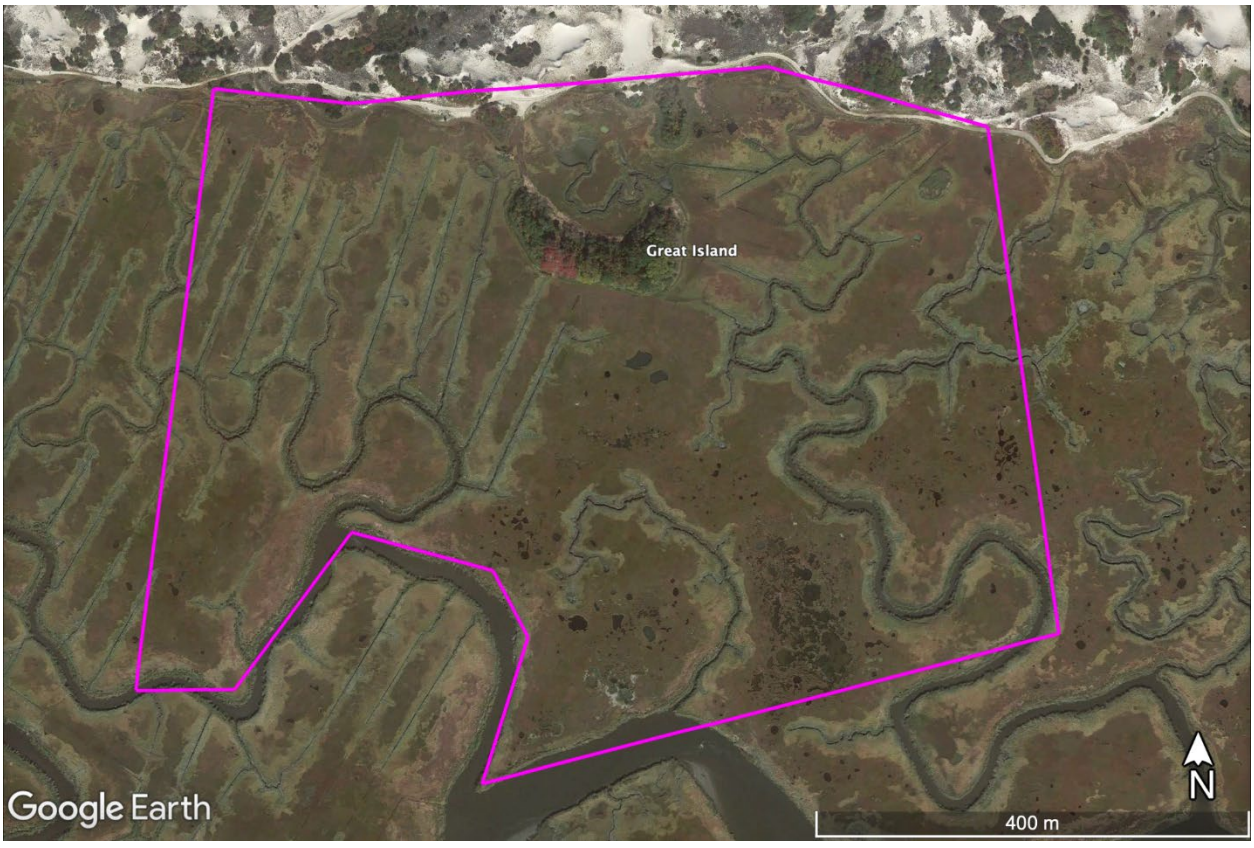

Figure 1 - Reconfigured Barnstable site boundary

Additional Training Data

Additional training and validation data (transect sampling) for classification models were acquired at some of our sites (Table 1). We collected additional data at sites where certain vegetation subclasses were not adequately represented in the training data from previous ground surveys. While in the field, we updated the classification of areas previously used for training if there was evidence that the plant community had changed.

Table 1 - Number of newly acquired training transects and polygons by field site

Site Name	Number of Features
Old Town Hill	32
North River	79
Barnstable	132
Wellfleet Bay	15
Red River	38
Horseneck Beach	46

Figure 2 - Collecting vegetation data

Drone-based Photogrammetry Products by Site

Figure 3 - Pre-flight check for the Matrice 600 drone

Table 2 and Table 3 present data on the number of data products produced for each field site from the beginning of the project through the end of the year, 2022. Table 4 and Table 5 provide data layer counts for orthomosaics and Digital Elevation Models (DEMs) acquired and developed since our previous project report was submitted (July 2021).

Table 2 and Table 4 provide counts of aerial image orthomosaic layers or "bands" from drone flights using various sensors (true color red, green, and blue, as well as sensors capturing non-visible light, such as Red-edge, NIR, and SWIR). These orthomosaics – produced using photogrammetry processes described in QAPP Appendix A – were used as inputs for salt marsh land cover classification modeling.

Table 3 and Table 5 provide tallies of DEM products produced through photogrammetry processing (described in the next section). The three column headings represent different drone-based sensing technologies used to develop the DEMs: 1) multispectral, our Red-Edge five sensor device, 2) RGB, a true color camera, and 3) LiDAR, a Light Detection and Ranging device that was flown for only for a few of our sites. We use DEMs for inundation mapping and embankment identification.

Note in both cases (orthomosaics and DEMs), data products from the 2023 field season (such as the revised Barnstable location) are not reported in these tables as they were being produced at the time of this writing.

Table 2 - Number of orthomosaic data layers by sensor type from project start through 2022

	Blue	Green	Red	Red-edge	NIR	SWIR
Old Town Hill	25	25	25	25	25	7
Essex Bay	26	26	26	26	26	9
Peggotty Beach	19	19	19	19	19	11
North River	7	7	7	7	7	3
South River	5	5	5	5	5	0
Barnstable	0	0	0	0	0	0
Wellfleet Bay	11	11	11	11	11	9
Red River	23	23	23	23	23	13
Horseneck Beach	21	21	21	21	21	7

Table 3 - Digital Elevation Models (DEMs) produced from project start to year-end 2022

	Multispectral Photogrammetry DEM	RGB Photogrammetry DEM	LiDAR DEM
Old Town Hill	14	7	2
Essex Bay	15	5	0
Peggotty Beach	12	3	0
North River	3	2	0
South River	4	0	0
Barnstable	0	0	0
Wellfleet Bay	5	4	2
Red River	6	5	2
Horseneck Beach	8	5	1

Table 4 – Orthomosaic images produced during this reporting period (July 2021 through year-end 2022)

	Blue	Green	Red	Red-edge	NIR	SWIR
Old Town Hill	13	13	13	13	13	6
Essex Bay	7	7	7	7	7	3
Peggotty Beach	6	6	6	6	6	4
North River	3	3	3	3	3	3
South River	2	2	2	2	2	0
Barnstable	N/A	N/A	N/A	N/A	N/A	N/A
Wellfleet Bay	6	6	6	6	6	4
Red River	9	9	9	9	9	5
Horseneck Beach	6	6	6	6	6	3

Table 5 - Digital Elevation Models (DEMs) by sensor type used to create the models, produced during the reporting period (July 2021-year end 2022). RGB data from 2022 exist for Peggotty Beach and South River, but those layers had not yet been processed.

	Multispectral Photogrammetry DEM	RGB Photogrammetry DEM	LiDAR DEM
Old Town Hill	3	3	2
Essex Bay	3	1	0
Peggotty Beach	4	0	0
North River	1	1	0
South River	2	0	0
Barnstable	N/A	N/A	N/A
Wellfleet Bay	3	2	2
Red River	1	2	2
Horseneck Beach	4	2	1

Digital Elevation Models, Digital Terrain Models and Canopy Height Models

As noted above and in Table 3 and Table 5, DEMs were produced from photogrammetry at all sites (except the reconfigured Barnstable site), and with LiDAR at a select number of sites. A description of the process for producing DEMs from LiDAR is described later in this document.

All DEMs were produced from low and mid tide imagery. DEMs produced with photogrammetry have been created from both multispectral and RGB imagery. The true-color Red, Green, Blue (RGB) photogrammetry DEMs have a higher spatial (cell size) resolution than the DEMs produced from the Red-Edge sensor's multispectral photogrammetry. Thus, the RGB models are preferred for site analysis in most circumstances. They are also more efficient to produce because of more reasonable equipment costs.

Importantly, DEMs represent the elevation of the surface of the vegetation canopy, water, or exposed soil. DEMs are not the same as Digital Terrain Models (DTMs), which represent the elevation of the land surface (i.e., the marsh 'platform'). We developed DTMs by flying drone-based RGB and selected LiDAR flights early in the growing season when plant biomass was at its seasonal low point. This maximizes exposure of the ground surface. Additionally, filtering processes such as Cloth Simulation Filtering (CSF) (Zhang et al., 2016), discussed at length later in this report, were applied to early season RGB and LiDAR models to produce DTMs that best represent elevation of the marsh platform.

Through filtering processes, we are able to produce RGB DTMs that are of similar accuracy (RMSE) to those produced with LiDAR. For inundation mapping at sites that do not have LiDAR models, we plan to use filtered RGB models. We have also used the CSF filtering process to produce canopy height models (CHMs); models that solely represent the height of the vegetation above the ground. We plan to use CHMs as part of the land cover classification process.

Salt marsh classification mapping: data analysis and modeling

In the time since our last report, we have continued to develop and refine our methodology for land cover classification mapping of salt marsh study sites. For details on data collection and processing procedures, see our previous report (Jackson et al., 2021) and QAPP. We obtained and integrated new aerial imagery data collected over the last two years, and collected new land cover training data. For the land cover classification, we aim to produce a classification for each site that includes three classes and up to 22 subclasses (see Appendix B) using primarily, if not exclusively, spectral values from the six spectral bands. We collected aerial images in the Red, Green, Blue, Red-Edge, Near-Infrared (NIR) and Short-Wave infrared (SWIR) bands. These aerial data were collected at various tidal stages and various time points over the course of the spring, summer, and fall seasons, and are spectrally calibrated to account for varying light conditions and to estimate at-surface reflectance in each of these bands. The intent was to collect data under a variety of conditions: at different tidal stages within a given day, at different stages in the lunar cycle (i.e. across different stages of the spring and neap tide cycle), and at different stages across a full growing season. Using aerial imagery from various tidal stages allows us to collect data on flooding patterns, and using aerial spectral data at different times throughout the season allows us to develop classification schemes informed by the phenology of salt marsh plants. As noted earlier, UAS-collected LiDAR data allowed us to create CHMs – representations of the height of various salt marsh vegetation – that may also prove useful for developing accurate land cover classifications for each of our salt marsh study sites.

It takes about an hour to collect aerial data in all bands for a 100-acre region. Images collected during each of these periods were combined into a multiband orthomosaic using photogrammetry techniques. These mosaics then undergo a Quality Assurance/Quality Control (QA/QC) protocol to ensure that they are of high enough quality (e.g., no blur, photogrammetry produced striping, etc.), sufficiently consistent, and unbiased enough to be used in land classification models. Orthomosaic raster layers that meet QA/QC standards are then parsed into individual bands for each of the flights and all bands from all time points are stacked into a single multiband – and very large – orthomosaic file. This single multi-band raster file is the primary input used by our classification models. While there may be gaps in the raster data in a few locations, pixels for any given site typically have over a hundred bands; that is to say, there is a vector of 100+ elements deep for each pixel used for classification models. Polygons of specific regions of salt marsh that had been classified either via ground-truthed data collected in the field or that were classified via photo interpretation were passed to the classification models for training and testing of model accuracy and errors (Figure 4).

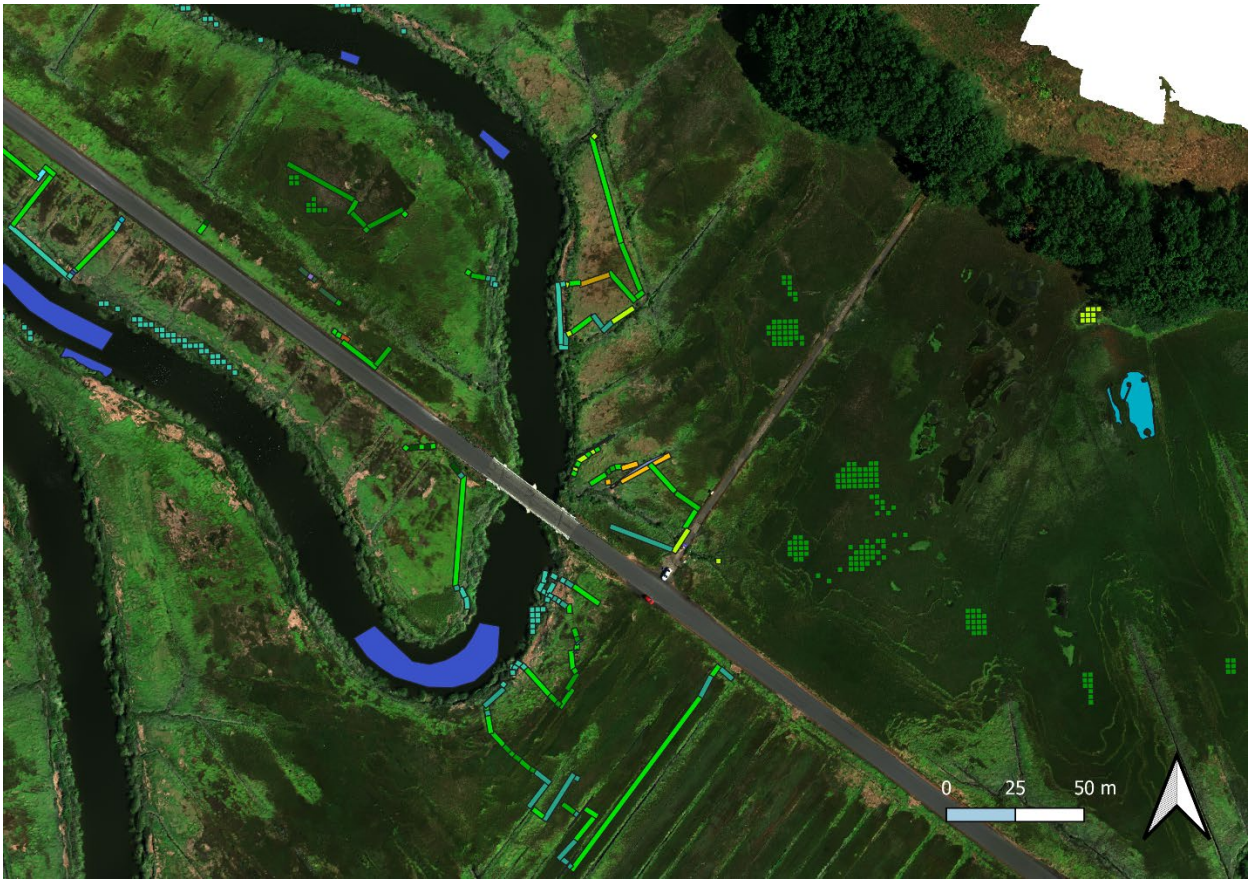

Figure 4 - An RGB (true color) image of a portion of the Old Town Hill study site showing strip transects and polygons from which training data were collected

An important takeaway from the above paragraph and the reference to "...over 100 elements deep for each pixel" is that the image stack used for land cover classification modeling for any of our study sites is substantial. Perhaps the most significant challenge we have had over the last two years is finding the computing power to handle such a substantial dataset. We use a Random Forest Modeling (RFM) approach to produce land cover classifications, and we have discovered that the computational requirements to run these models with these full stacks of data are quite high. Consequently, over the last two years we have had to get creative to find a computational platform that can handle the modeling demands (our initial computing platform that we used for orthomosaic creation turned out to be underpowered for this modeling task). We began using a high-performance computing cluster with access provided through a multi-university consortium. However, due to circumstances outside of our control, that platform eventually became unavailable for our modeling efforts. After some significant time exploring other computational platform options, we settled on a high-performance computing cluster called "Unity" that exists to support research teams from the University of Massachusetts Amherst, University of Massachusetts Dartmouth, and the University of Rhode Island. After some significant effort learning how to operate and program on Unity, we developed scripts that allowed us to successfully run Random Forest Models (RFM)[1] using the data stacks we generated for our study sites. Figure 5 below shows the output of one such model run, on our Old Town Hill study site.

[1] We are now exploring the use of another modeling approach, called "XGBoost" as an alternative to the typical RFM approach.

Standard Random Forest Models (RFMs) versus Iterative RFMs

While initial classifications using RFM Version 1 (RFM v1), like the one shown in Figure 5, had a high degree of accuracy, there were also significant errors of commission and omission for many of the subclasses. Our team spent much time analyzing these initial land cover classifications, and through that process, we gained insight on ways to refine our classification modeling approach. In some cases, certain land cover classes in our scheme might look spectrally similar but represent regions of a marsh that differed significantly in elevation and tidal dynamics.

For example, Subclass 01, which was classified on the ground as being dominated by tall-form *Spartina Alterniflora*, was occasionally classified by our model as Subclass 09, a classification that includes a significant amount of shrubs such as *Iva Frutescens* and *Baccharis Halimifolia* (Figure 6). In another area of the marsh, portions of salt marsh identified on the ground as Subclass 06 (dominated by *S. Patens* and *Distichlis Spicata*) were classified by our model as Subclass 09 (Figure 7).

Another set of subclasses for which we noticed significant confusion in our RFM was between tall-form *S. alterniflora* dominated subclasses (Subclasses 1 and 2) and a *Phragmites australis* dominated subclass (Subclass 12). The former occupies low and intermediate marsh while the latter tends to occur on the high marsh where there is an influx of freshwater. It is important that we are able to distinguish between these two types of vegetation. From the air, under certain conditions during a season, those two species can look somewhat similar, although a trained photo interpreter generally would be able to distinguish the two, if by nothing else than understanding the regions in a marsh where those species tend to occur. There is an advantage however to having the classification work exclusively from spectral, seasonal and temporal information for each pixel without considering context.

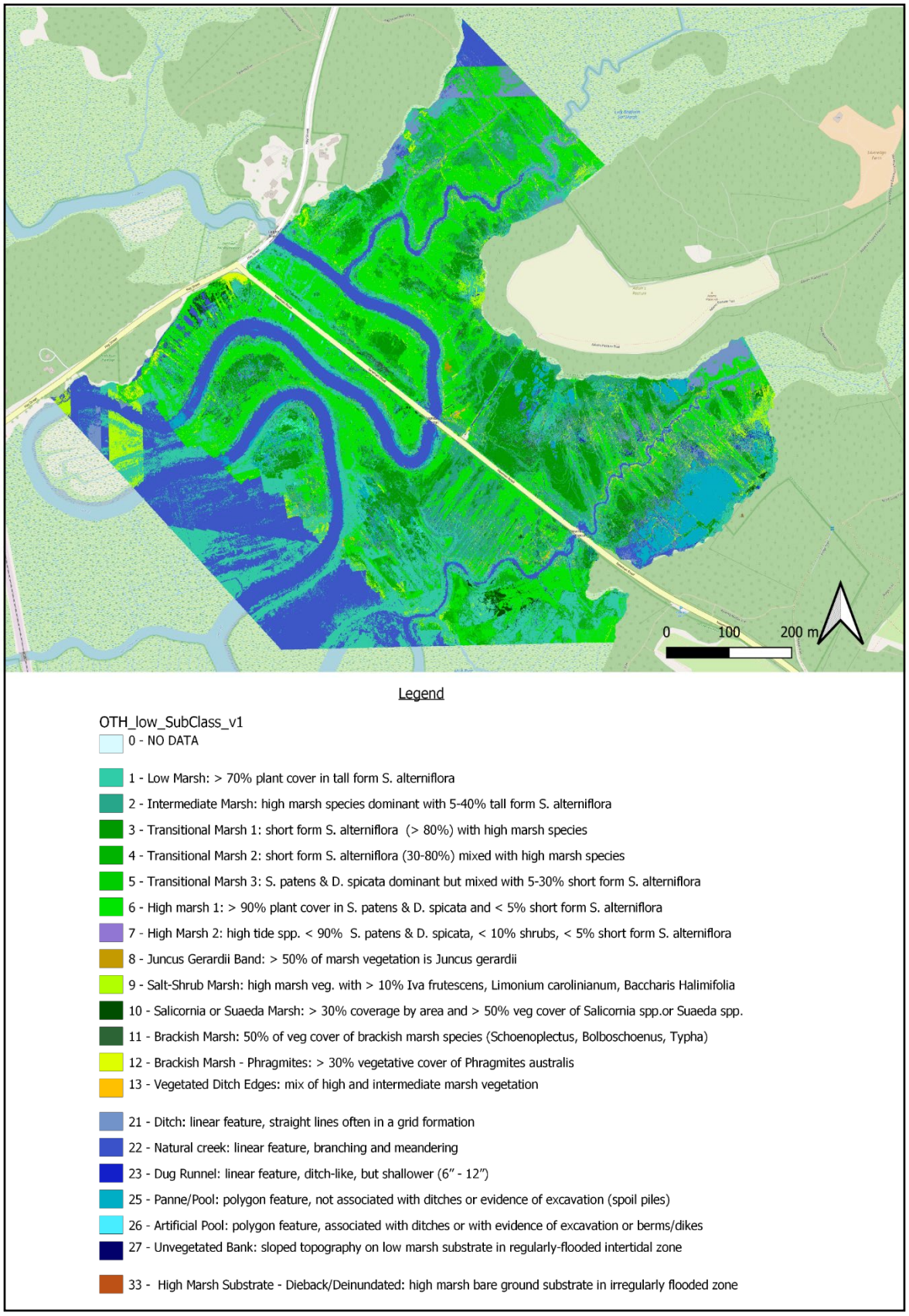

Figure 5 - Old Town Hill classification using Random Forest Model (RFM) v1: All Subclasses

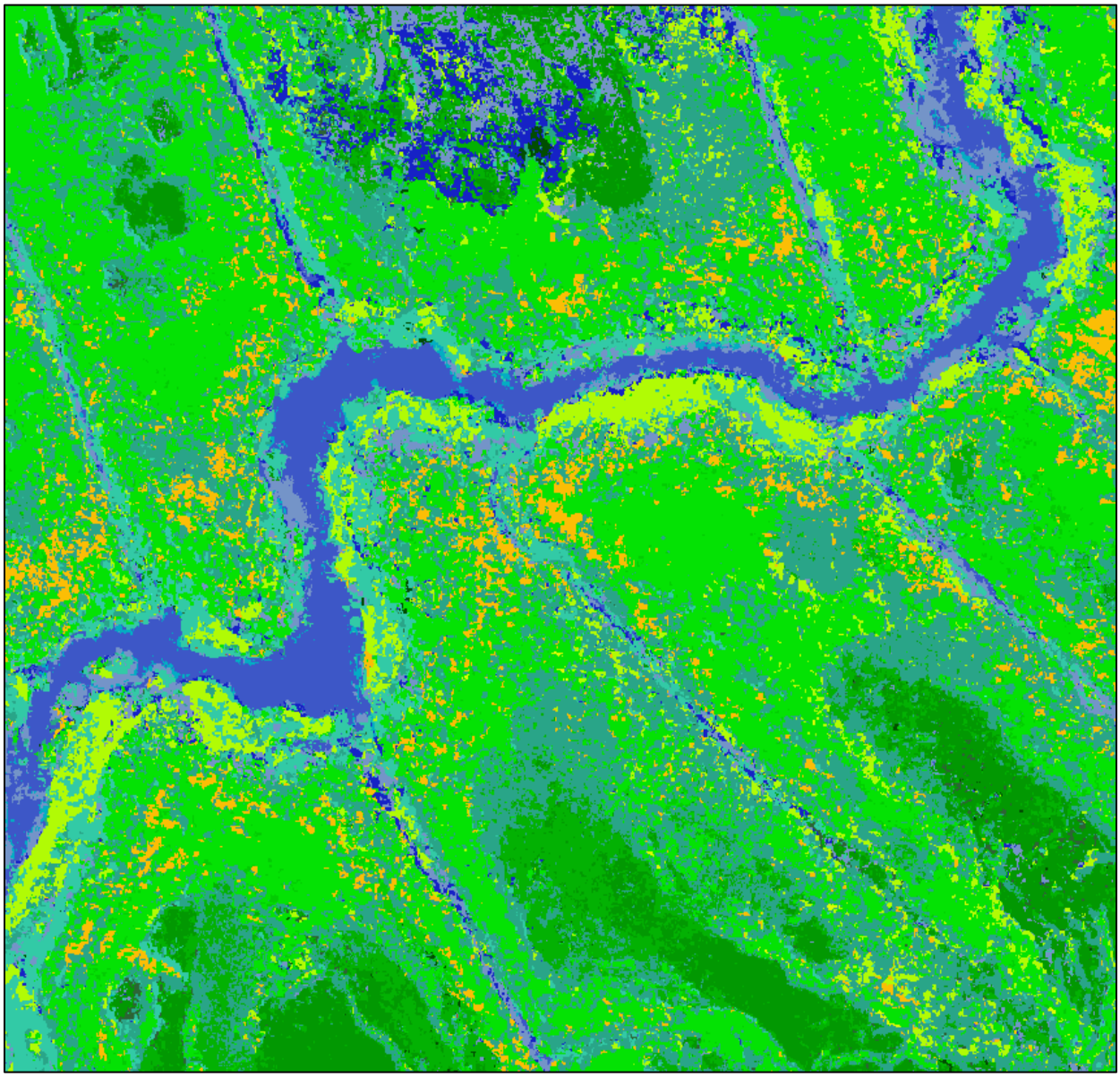

Figure 6 - Along the southern banks of this creek, we can see regions of brighter yellowish-green, indicating the vegetation here was classified as Subclass 09 (shrub marsh). In reality, these are regions of Subclass 01 (tall-form S. alterniflora*). Subclass 09 is typically associated with high marsh, while Subclass 01 is considered low marsh. The misclassification is an example of errors of commission for Subclass 09, and errors of omission for Subclass 01. While errors of omission for Subclass 01 are relatively small, some regions, like this one, were incorrectly classified; in fact, they were assigned to a subclass that typically occurs at nearly the opposite end of the salt marsh's hydrological range.*

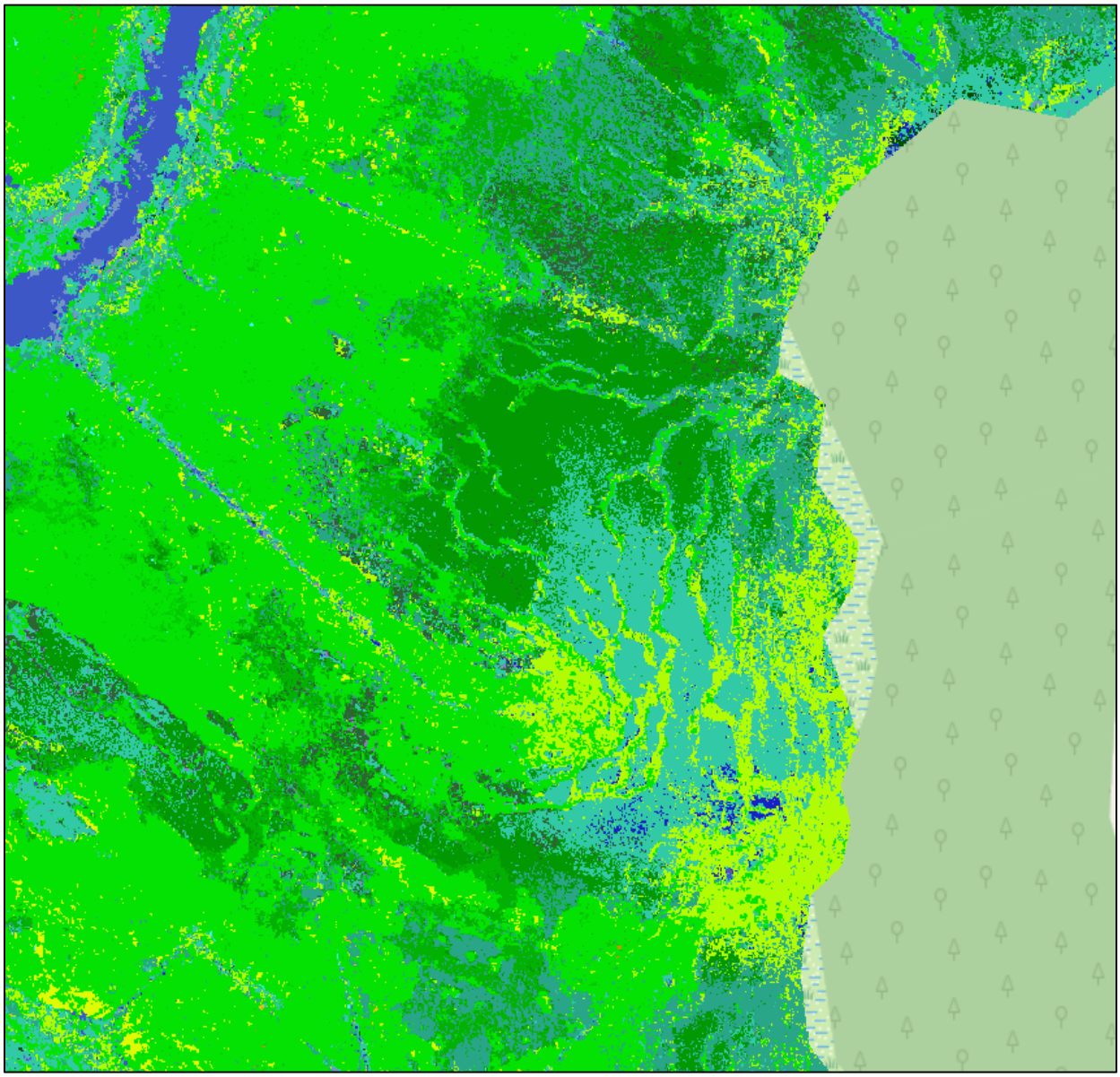

*Figure 7 - Here the streaks of yellowish-green indicate regions that have been classified as Subclass 09 (shrub marsh), when in reality those regions are distinctly Subclass 06 (*S. Patens *and* D. Spicata *dominant). While both of these vegetation types are generally found at higher elevations within a salt marsh, they typically represent areas with different sediment or tidal hydrology, and the plants themselves are quite different ecologically. The misclassification is an example of an error of commission for Subclass 09, and an error of omission for Subclass 06.*

While the Random Forest Modeling produced classifications that are mostly accurate, our examples above suggest that there is room for improvement. Over the last two years, we have investigated alternative strategies for improving classification results.

The first strategy employed an “Iterative Classification Scheme” (ICS) using a piecewise iterative classification approach. For an ICS we use RFM or XGBoost to first classify the land cover into classes (i.e. water, vegetated land, and bare ground; Figure 8). We then proceed to classify aggregate groups of subclasses within their appropriate class, and then subsequently classify the subclasses within their appropriate aggregate subclass group. The intent was to cluster subclasses in a way that constrains the RFM and reduces the misclassification of subclasses among aggregate subclass groups (such as confusing

Subclasses 6 and 9, Subclasses 1 and 9, or Subclasses 1 and 12). In this iterative process, once we isolated vegetated cover as shown in Figure 8, we could then run subsequent classifications for more specific groups of subclasses - or specific subclasses themselves - exclusively within the vegetated region.

Iterative Classification Scheme Version 3 (ICS v3)

For one of our early attempts in exploring this ICS approach (ICS v3, Figure 9) the second classification step used RFM to classify the vegetation class into subclasses 3 and 13 (and a new subclass, 99, for trees along the marsh border), and aggregate groups that included all other vegetation subclasses. If this second step showed improvement over RFM v1 the aggregate groups could then be separated into appropriate subclasses. Figure 9 outlines the iterative approach for achieving a vegetated land cover classification for every subclass.

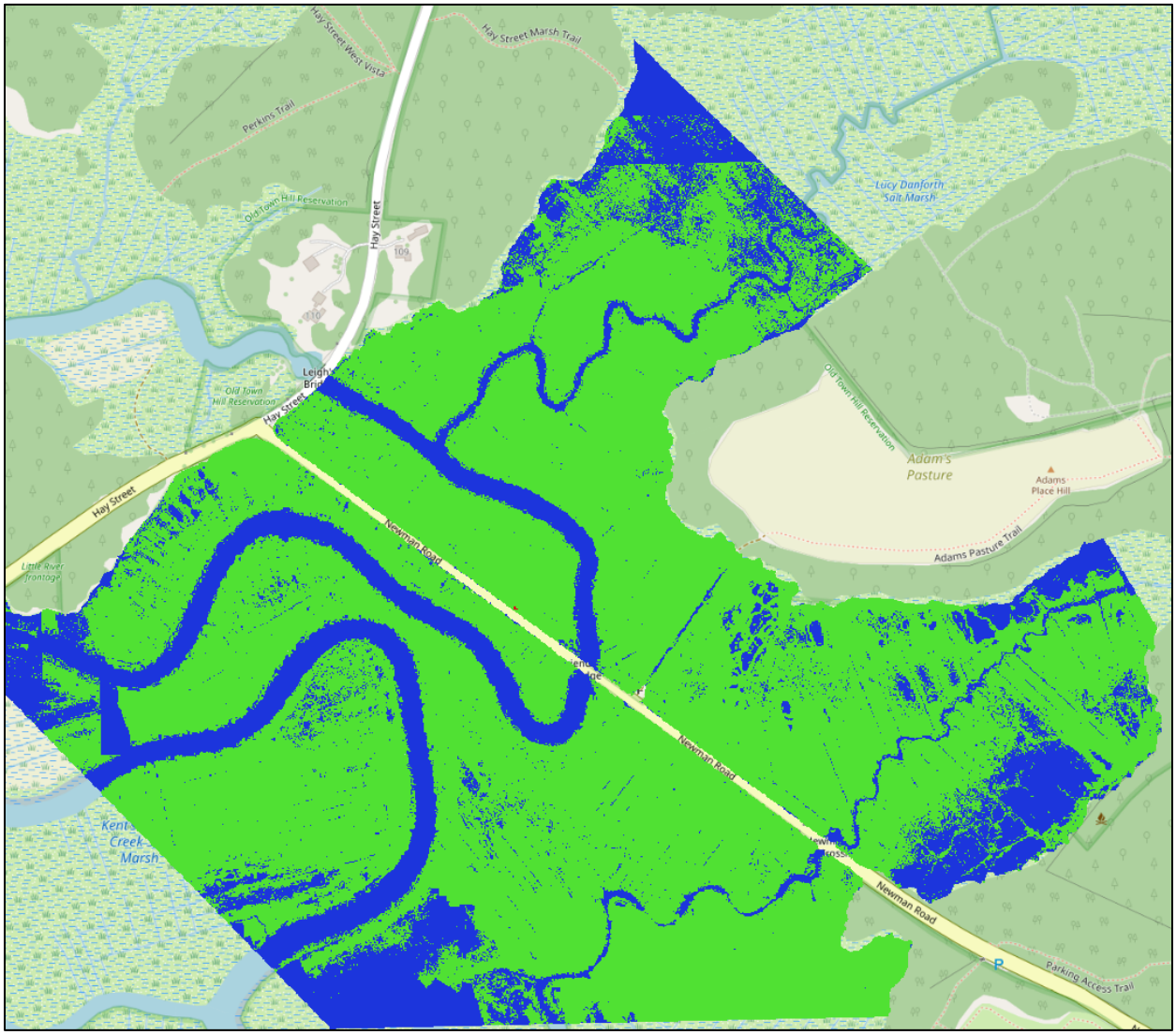

Figure 8 - Classification of Old Town Hill using a Random Forest Model (RFM), where the classification goal was strictly to classify the site into land features vs water features. Here the green extent indicates regions that have been classified as vegetated land cover, whereas the blue extent indicates regions that have been classified as water features.

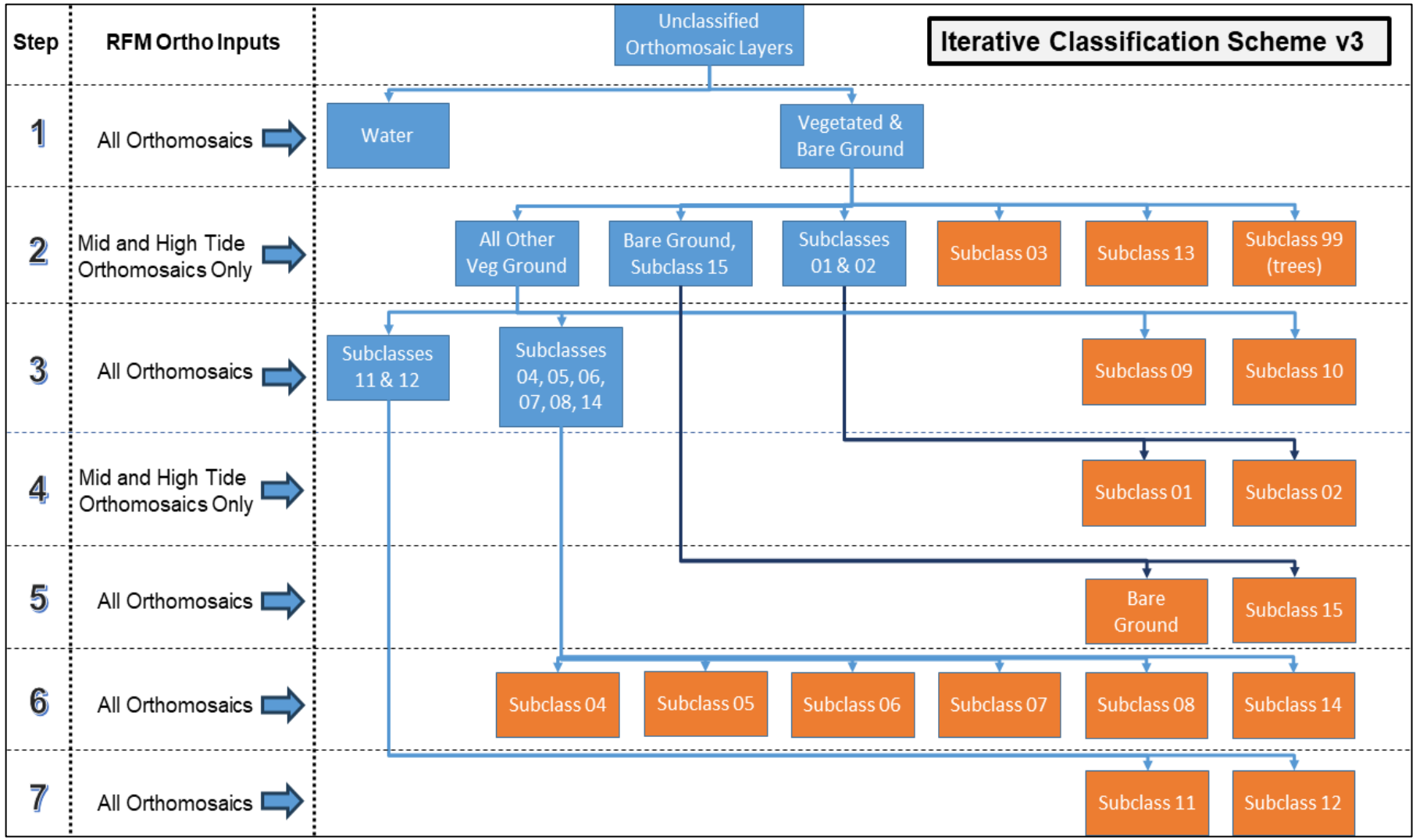

Figure 9 - This diagram illustrates an iterative classification scheme for ICS v3. In this diagram, the sequential classification steps are listed 1-7 from top to bottom. The specific subclasses or groups of subclasses that we aim to have the RFM successfully classify at each step are in labeled boxes for each step, where blue boxes represent groups of subclasses, and each orange box represents a single specific subclass. The arrows connecting each of the boxes represent the regions over which we ran the RFM classification for that particular step. For instance, in step 3 the RFM to classify regions of Subclass 09 and Subclass 10 respectively was applied only in regions that had already been identified as "All Other Veg Ground" in step 2. The orthomosaic inputs for each step are shown in the "RFM Ortho Inputs" column.

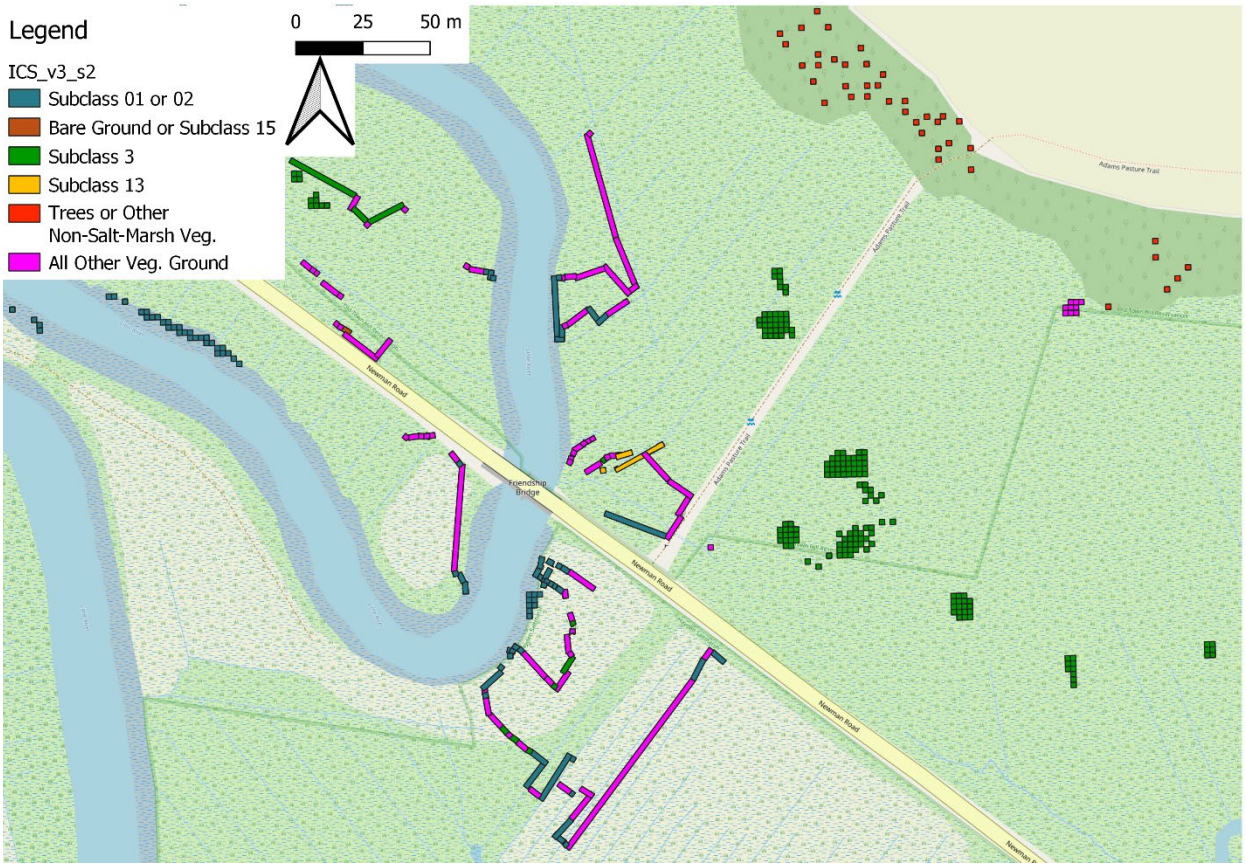

Figure 10 - Iterative Classification Scheme Version 3 (ICS v3). In this image, we show how we grouped the training data (strip transects and polygons) for the second step of ICS v3.

We are using a variety of ICS schemes for classification to maximize the accuracy of vegetation mapping. How we group subclasses, what training inputs we provide the RFM at each step, and in what sequence we attempt to differentiate between these groups can be expected to affect the final classification results. Figure 10 provides an example of how we initially grouped training data to support ICS v3 (Figure 9). Focusing first on Subclasses 1, 2, 3, and 13 allowed us to address model confusion involving vegetation types that typically occupy very different areas of a salt marsh. Confusing land cover subclasses that often occur in similar regions of salt marsh, such as Subclasses 4 and 5 was not a significant concern at this stage in the process. We expect that the different regions of the salt marsh (low marsh, high marsh, border marsh, brackish marsh) will be easier to distinguish from each other by relying on the mid-tide and high tide orthomosaic layers as inputs into the RFM. Lower regions (low marsh) are likely to be flooded during mid tide and high tides while other regions are not expected to be flooded at mid tide and would likely be flooded by only shallow water or no water at all during high tides. This should help us identify and distinguish among those groups of subclasses.

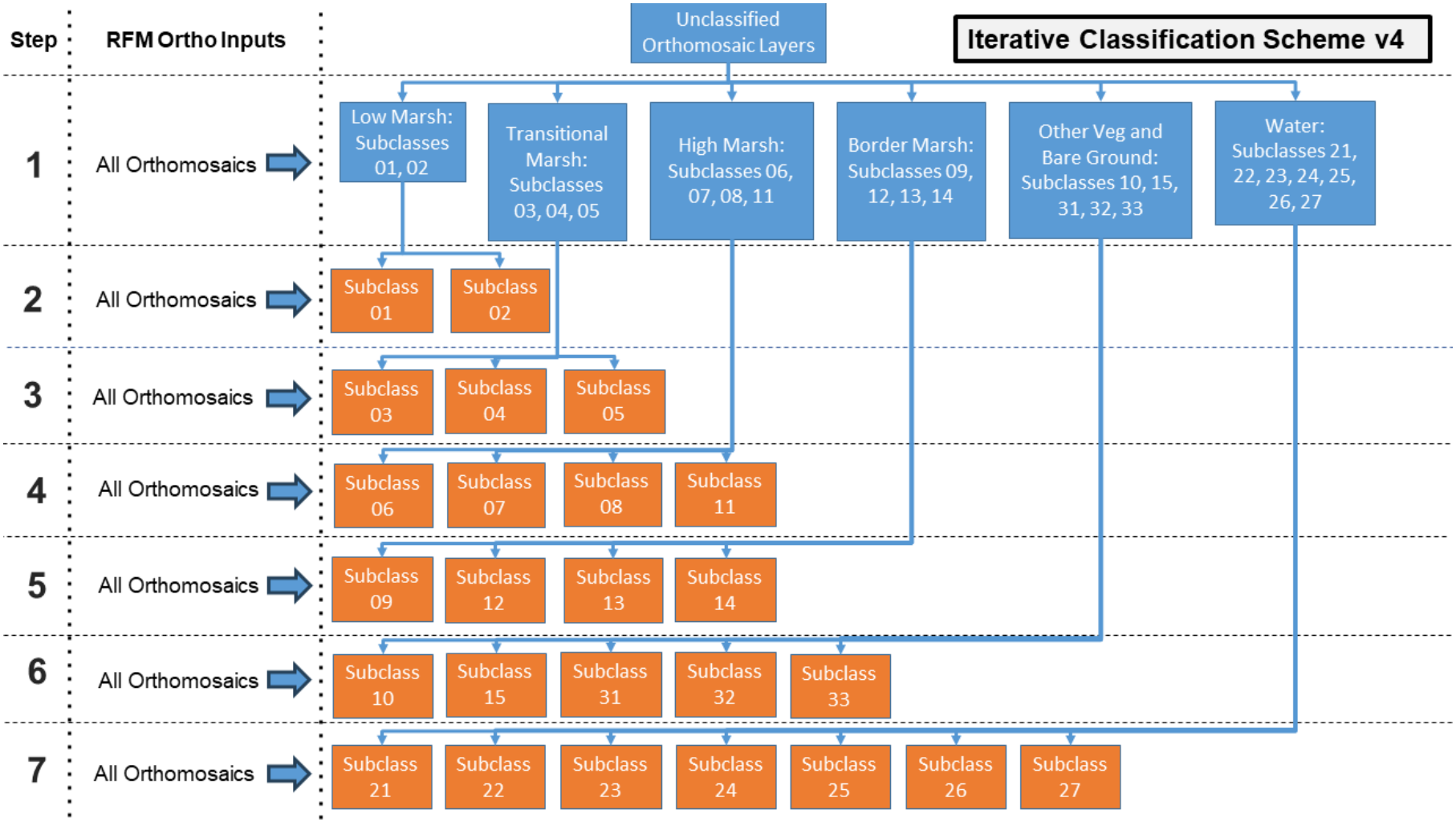

Figure 11 - This diagram illustrates Iterative Classification Scheme Version 4 (ICS v4). In this diagram, the sequential classification steps are listed 1-7 from top to bottom. The specific subclasses or groups of subclasses that we aim to have the RFM successfully classify at each step are in labeled boxes for each step, where blue boxes represent groups of subclasses, and each orange box represents a single specific subclass. The arrows connecting each of the boxes represent the regions over which we ran the RFM classification for that particular step. The orthomosaic inputs for each step are shown in the "RFM Ortho Inputs" column.

Iterative Classification Scheme Version 4 (ICS v4)

Figure 11 outlines Iterative Classification Scheme Version 4 (ICS v4), where the subclasses are grouped differently, and the RFM inputs are selected somewhat differently, than in ICS v3. Rather than classifying just a few particular subclasses in the second classification step (except for trees - i.e., non-salt marsh vegetation) as ICS v3 does (Figure 9 and Figure 10), this iterative classification scheme balances each of the classification steps and subdivides all subclasses into aggregated groups of subclasses before focusing on the individual subclasses. In ICS v4, step 1 aggregates all of the salt marsh vegetation subclasses into six groups (Figure 12):

1. Water
2. Low Marsh or Intermediate Marsh
3. Transitional Marsh
4. High Marsh A
5. Border Marsh
6. Other Vegetation or Bare Ground

We based these groupings on the visual distinctiveness of subclasses; subclasses with similar visual characteristics in the aerial imagery were grouped together. These groupings also tended to share similar hydrological characteristics, although this is not true in all cases.

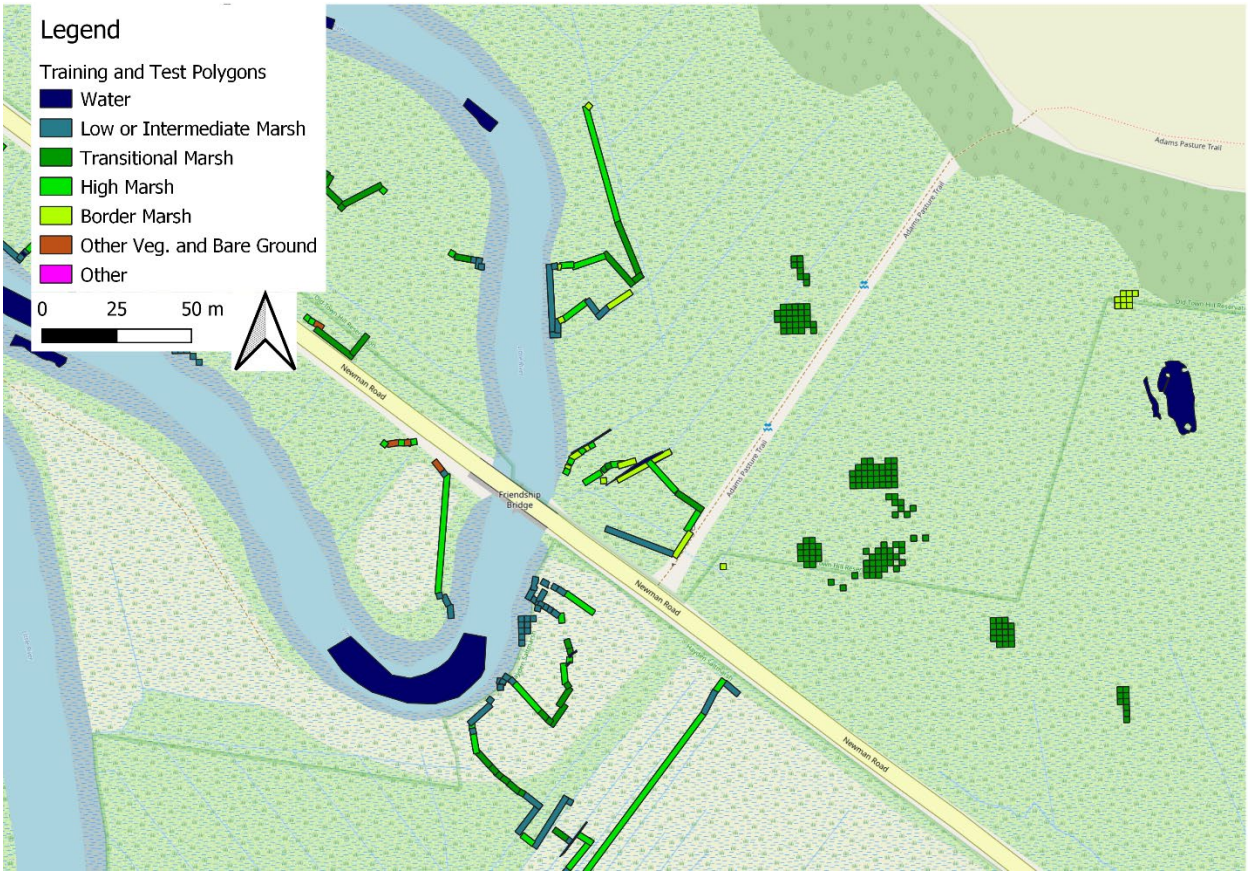

Figure 12 - The reclassified training data for the first step in ICS v4

We are still exploring in an effort to determine what specific ICS will achieve the most accurate classification. In ICS v3 most (10) of the subclasses are grouped together into one of the aggregate subclass groups at step 2; two other aggregate groups each contains two subclasses, and two individual subclasses are classified at this step. ICS v3 uses high tide and mid tide imagery to take advantage of a higher spectral contrast between flooded and non-flooded vegetation types. However, this imbalance in the aggregate subclass groups means that the one large group contains a higher amount of spectral variability, and that relatively larger variability could give rise to significant errors of commission or omission. ICS v4 has a more balanced grouping of subclasses that are segregated based on the spectral attributes of the subclasses. Because of this, we hypothesized that ICS v4 might do a better job of minimizing errors of commission and omission among the groupings at the first step, but not necessarily overall.

As an example of how subtle changes in the ICS can yield significantly different results, ICS v4 removed the subclass “Trees” for the model training set, whereas ICS v3 included it in step 2. We added the “Trees” subclass and training data in ICS v3 to help the model differentiate between trees and high marsh vegetation (especially *P. australis*) along the border of the salt marsh. While this still may be a useful feature in our final model, we found that introducing a “Tree” subclass into ICS v3 resulted in errors of omission due to areas of salt marsh being classified as trees, at least at an early step of the ICS. ICS v3 attempted to distinguish trees in step 2, whereas ICS v4 does so at a later step. Introducing the “Trees” subclass and training data at step 2 of ICS v3 produced errors well into the interior of the salt marsh, even as far as the transitional marsh. We believe that we can prevent these errors by identifying areas of transitional marsh before we introduce the “Trees” subclass into the model.

Comparing ICS v3 and ICS v4

While the initial RFM classification (RFM v1) works reasonably well in most areas, there are some areas that were incorrectly classified. Figure 13 shows a portion of the Old Town Hill site. In the eastern quarter of the figure, some of the areas in light green-blue were incorrectly classified as low-marsh vegetation when in actuality this is an area of high marsh platform. This region is quite wet and short form *S. alterniflora* is dominant. Because this model uses only spectral inputs it is possible that the presence of short form *S. alterniflora* in such a wet environment is why the classification mistook this region for low marsh.

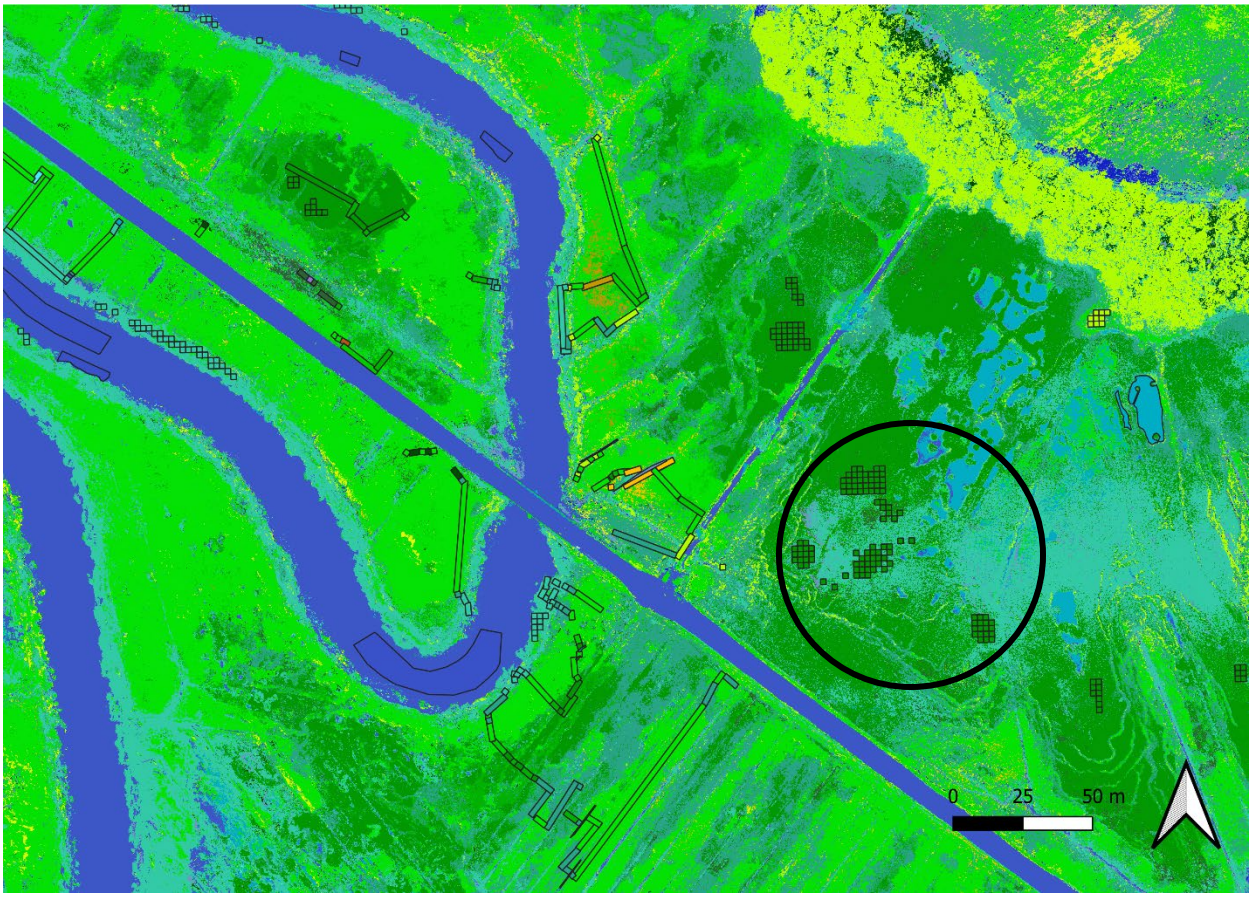

Figure 13 - Standard RFM Version 1 (RFM v1) with all subclasses individually classified. The color scheme to denote each land cover subclass is the same as in Figure 5. Strip transects and polygons from which training data were collected are shown using the same color symbology. The black circle identifies an area of misclassification.

If we compare ICS v3 with the results from the RFM v1 (Figure 14), at first glance it appears that a significant number of the errors in RFM v1 were correctly classified in ICS v3. Regions for which the RFM v1 had misclassified the marsh platform as low marsh appear to be correctly classified by ICS v3 as subclass 03 or as "all other vegetation" (white circles). However, an area in the northeastern portion of each image (white rectangles) was more accurately classified by RFM v1 (based on ground-truthing) than those same areas classified by ICS v3. A similar pattern was found when comparing RFM v1 and ICS v4 (Figure 15).

In Figure 16, the "all other vegetation" category for ICS v3 included some areas, such as an area along an eastern bank of the channel and along the western bank of the channel where it runs north-south, that should have been classified as low marsh (subclasses 1 or 2). We found that *P. australis* and *S. alterniflora* were occasionally confused in RFM v1 and this confusion may also be affecting ICS v3. With ICS v3, *P. australis* was grouped in a large, aggregate group "all other vegetation." This may be an example of where having an aggregate group of subclasses with a wide variety of spectral attributes increases the potential for that aggregate group to be overrepresented in the model classification. These same areas were correctly classified using the more balanced aggregation for ICS v4. We are continuing our efforts to find an approach that can address all these sources of errors within one classification model.

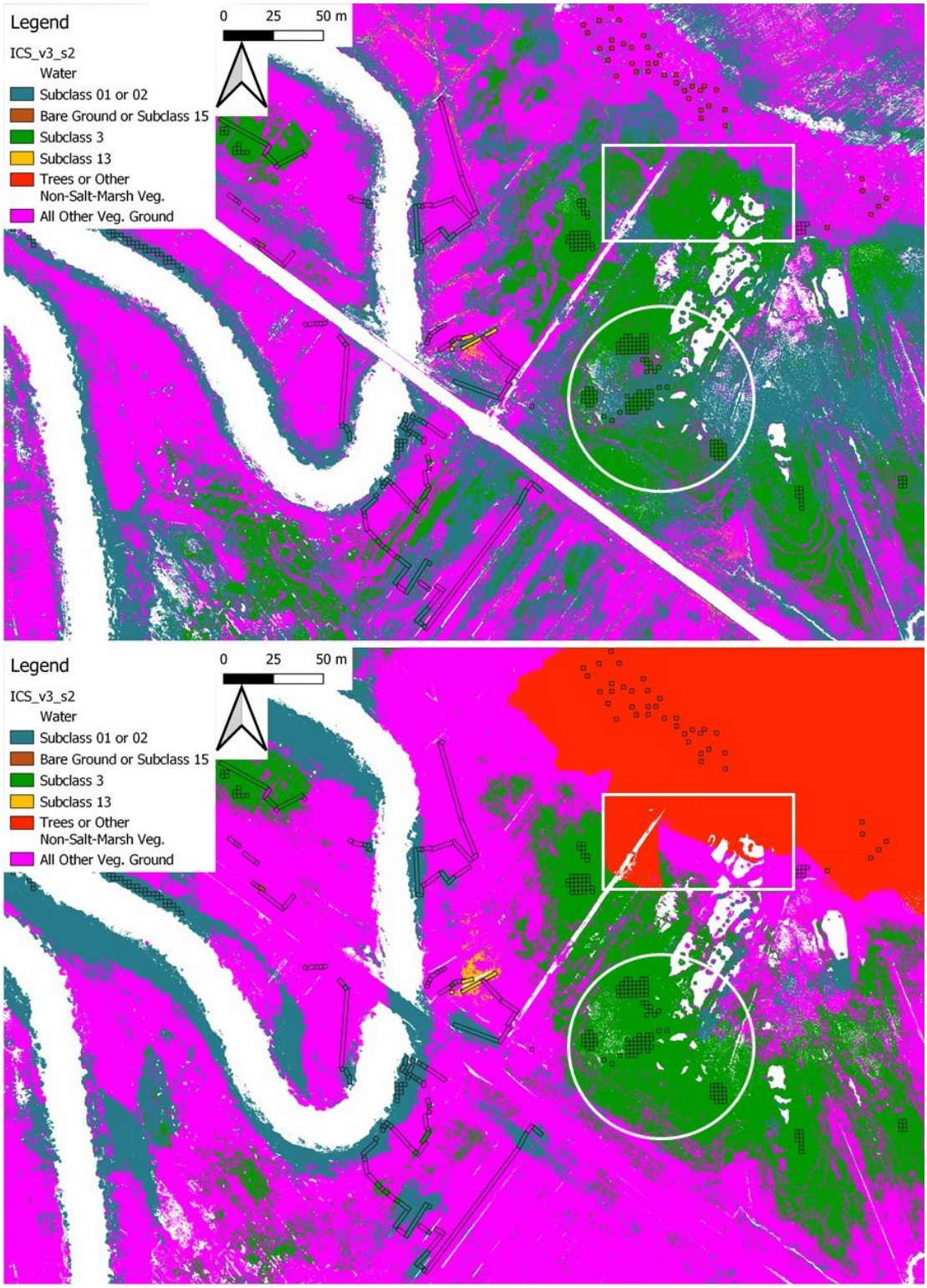

Figure 14 - An area of the Old Town Hill site with RFM v1 land cover reclassified to match ICS v3 (top) and the classification scheme ICS v3 after step 2 of the classification (bottom). Areas of water were masked out (those regions are mapped as white). Strip transects and polygons from which training data were collected are shown using the same color symbology. Areas in red represent areas modeled as tree and other non-marsh vegetation. Areas in magenta represent areas modeled in the aggregate group "all other vegetation," which includes marsh platform communities. The white circle identifies an area misclassified by RFM v1; the white rectangle is an area misclassified by ICS v3.

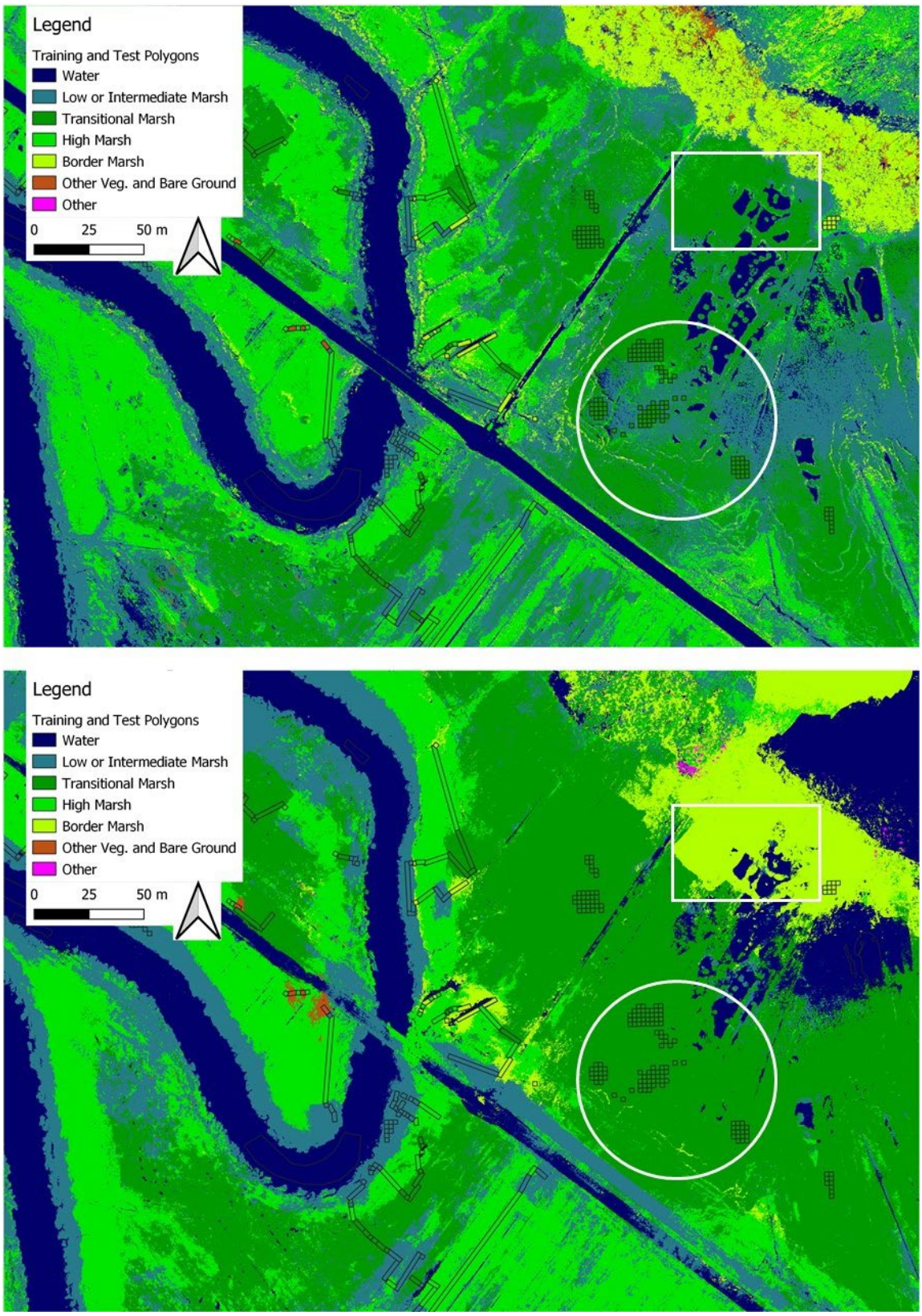

Figure 15 - An area of the Old Town Hill site with RFM v1 land cover reclassified to match ICS v4 (top) and the classification scheme ICS v4 after step 2 of the classification (bottom). Strip transects and polygons from which training data were collected are shown using the same color symbology. The white circle identifies an area misclassified by RFM v1; the white rectangle is an area misclassified by ICS v4.

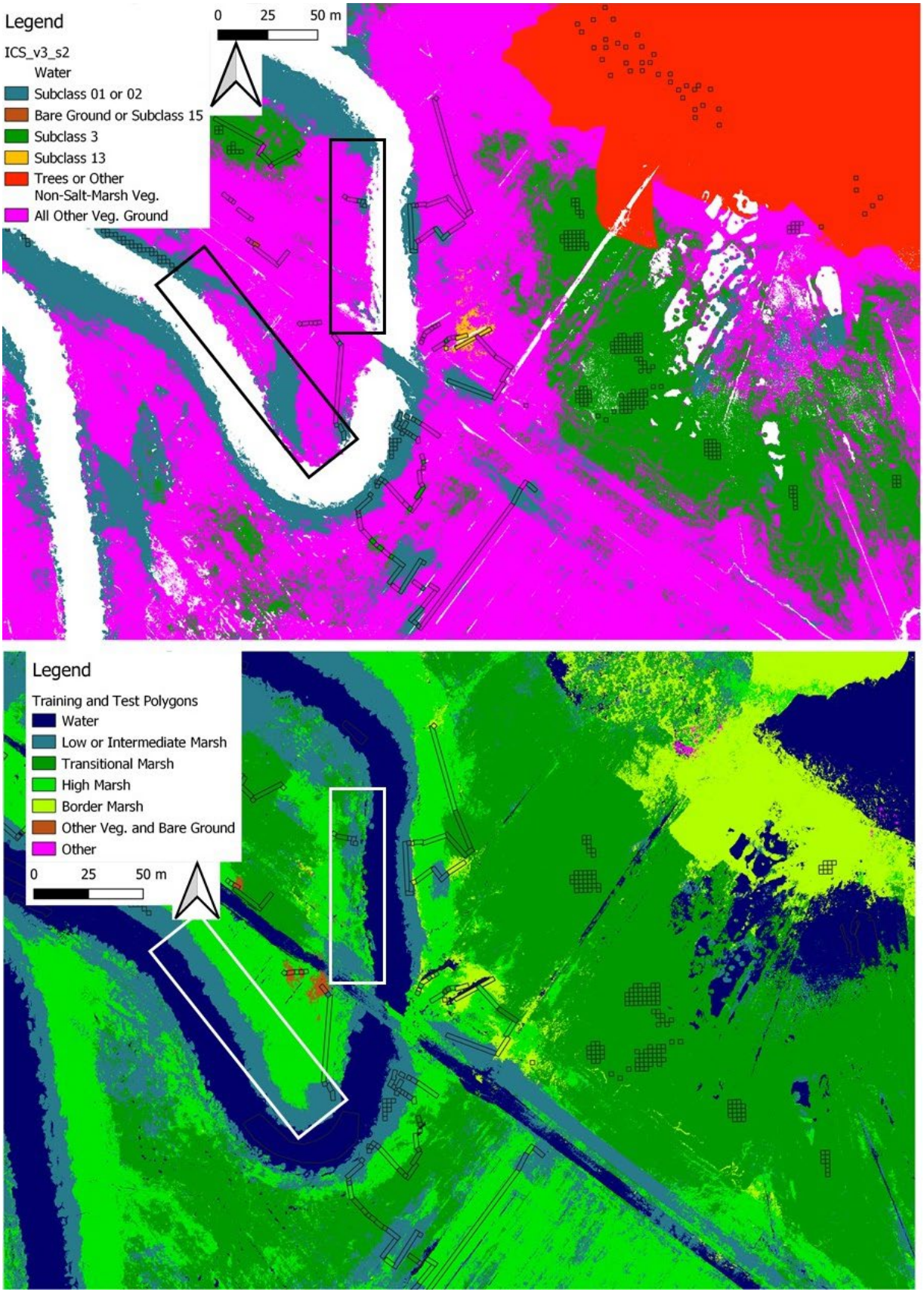

Figure 16 - Land cover classification for ICS v3 (top) and ICS v4 (bottom). Areas in rectangles are areas of low marsh vegetation misclassified by ICS v3 but correctly classified by ICS v4.

Summary

We have not yet determined if one or another of these ICS approaches will ultimately lead to a more accurate classification across subclasses. This is one of our main priorities to address in the coming months.

We will also be exploring other means of improving the land cover classification, such as:

1. Disaggregating spectral data and training data collected across all six years of data collection to avoid classification errors due to vegetation changes over time. We intend to test classification effectiveness using subsets of data from 1 or 2 year periods.
2. Aggregating training data across sites to increase representation for less common subclasses.
3. Adding CHMs as data inputs to the RFM. This will incorporate vegetation height into our models.
4. Testing the effectiveness of other classification models relative to the Random Forest Models (RFM).
5. Test the usefulness of publicly available LiDAR or spectral data sets for land cover classification inputs.

Insights gained from our experience with standard RFMs have led to adjustments that could potentially improve our classification accuracy. Once we have implemented and tested alternative classification models we look forward to sharing the results in a future report.

Beyond improving the land cover classification, the aim of testing these different approaches is to discern what data inputs are of the greatest importance to achieve a high level of accuracy. Our objective is to make the methodologies that we develop not just accurate, but also practical and cost-effective to implement. We are confident that this research will provide insights into what combination of aerial data and ground data collection are needed to accurately map vegetation, bare ground, and water features in salt marshes. We suspect that the distribution of vegetation communities in a salt marsh could then serve as an indicator of salt marsh condition and vulnerability to sea level rise.

Water Logger Arrays, Specifically Timed UAS Flights, and Inundation Mapping

Figure 17 - Water logger installation

Purpose

One of the key attributes that we seek to measure at the salt marsh study sites is flooding extent and flooding patterns. As we discussed in our prior report, near-infrared (NIR) and shortwave infrared (SWIR) imagery collected with our UAS equipment are well-suited for delineating a water-land boundary so long as there is an unobstructed line of sight to the features on the ground. In many salt marsh locations, this is adequate so long as the vegetation is short enough for the aerial imagery to detect the presence of surface water. In many salt marsh areas, where the vegetation is taller, the vegetation canopy obscures the substrate and interferes with our ability to detect standing water. Land cover classification schemes that work just with multispectral imagery often cannot see the dark features that would indicate the presence of water under dense vegetation even when we are quite confident that water is present. In part as a means of addressing this issue, and in part in a more general sense to supplement our aerial data collection and land cover classifications, we deployed an array of water loggers to better understand the tidal hydrology of our study sites (Figure 17).

Data collection

Prior to our use of water logger arrays, we had been deploying three water loggers at each site for each field season: one in a tree on the marsh edge to provide barometric calibration for pressure changes in the atmosphere, a second on the marsh platform, and a third deployed in a creek or channel to measure the approximate frequency of flooding and height of the water in each of these locations. Over the last two years, however, we deployed in each site an additional array of approximately 40 water loggers for 2 to 3-week increments during which we flew weekly flights at high tide. These arrays distributed water loggers at various locations within each salt marsh to measure the presence, depth, and duration of flooding at each location. We used four criteria for distribution of water loggers within the marshes (Figure 18).

1. Many of the loggers were placed along transects varying in elevation.
2. Loggers were placed in a variety of different land cover classes, with an emphasis on documenting tidal hydrology on the high marsh platform.
3. Loggers were distributed at varying distances from creek channels and ditches.
4. Transects and loggers were distributed across the site in a somewhat representative manner so that they were not all clustered in a particular region of the salt marsh.

All of the water loggers were synchronized to measure the depth of water every 10 minutes. As not all water loggers were at the same elevation - some were in creeks, some were on the platform, some were in ponds - there was variation as to what depth of water a water logger might report. The time series measurements that each water logger recorded were analyzed to determine how often it was exposed to surface water, for what duration it was exposed to surface water for each flooding event, and to what depth it was flooded for each flooding event. Thus far, we have collected data from water logger arrays at seven sites; we expect to complete data collection at our other two sites in 2024 (Table 1).

Table 6 - Deployment dates and number of water loggers used for each of our salt marsh study sites. The South River and Barnstable sites will be sampled in 2024.

	Deployment Dates	Number of Loggers
Old Town Hill	8/18/2022 to 9/8/2022	41
Essex Bay	7/7/2023 to 8/2/2023	40
Peggotty Beach	8/3/2023 to 8/28/2023	40
North River	8/31/2023 to 9/14/2023	40
South River	TBD	TBD
Barnstable	TBD	TBD
Wellfleet Bay	10/19/2022 to 11/23/2022	41
Red River	9/15/2022 to 10/7/2022	40
Horseneck Beach	7/21/2022 to 8/15/2022	42

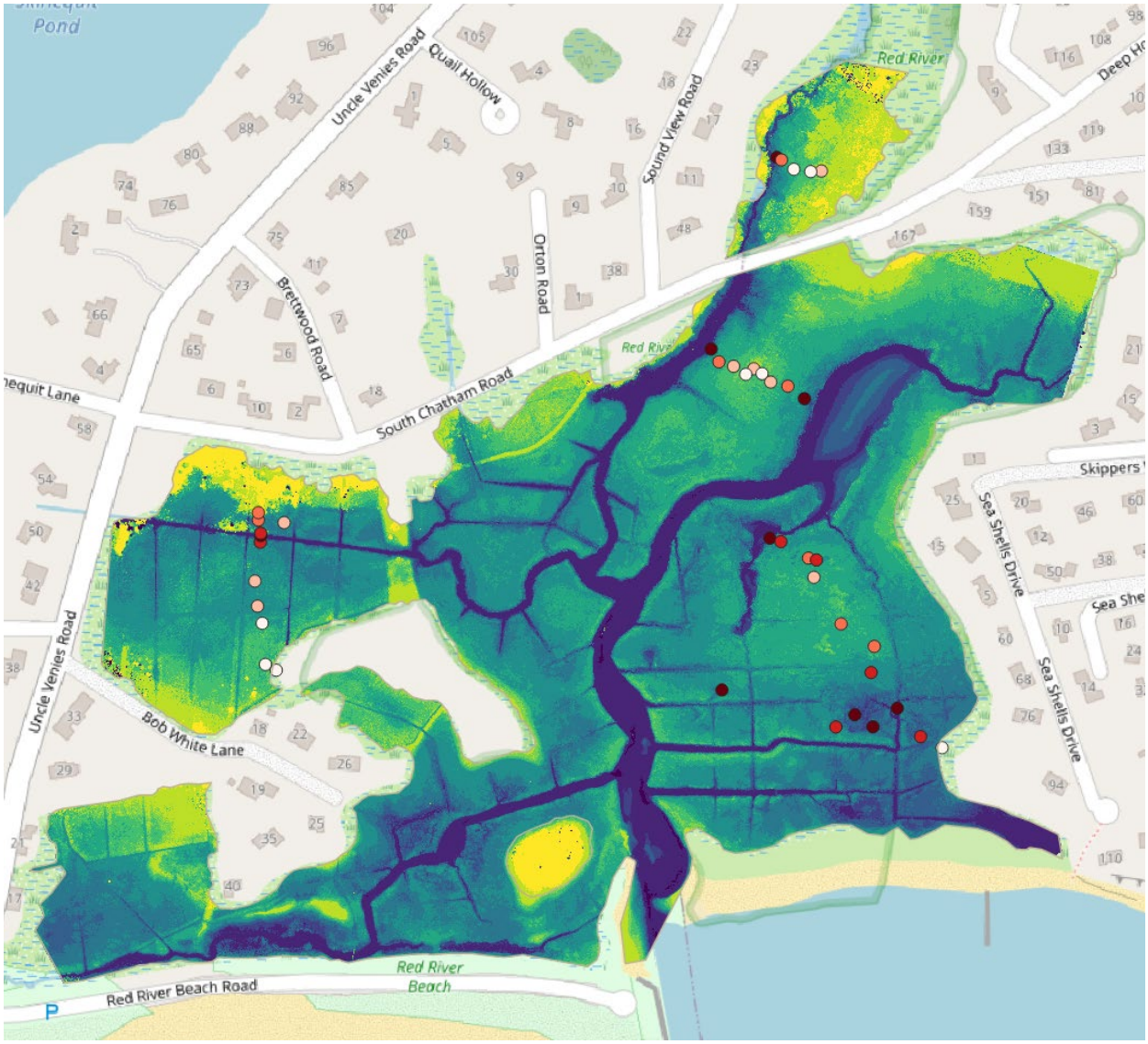

Figure 18 - Distribution of water loggers at the Red River site; the color map for the raster grid in the image represents elevation class (blue for lower elevation; yellow for higher elevation). Classes were determined by tighter clustering around modes of elevation across the site and water loggers were located in a variety of different elevation classes. Small circles on the map represent water logger locations, and the color scheme represents a combination of "proportion of time inundated" and "average inundation depth" (darker red represents greater depth of inundation).

Data Analysis

At seven of our sites, we placed an array of 40-42 water loggers, in a variety of locations, elevations, and vegetative classes. Our goal was to use this dataset of inundation, elevation, and date/time to estimate water movement over the marsh during a period of neap to spring tide. We began this analysis by focusing on one of our sites: Red River. We utilized Troy Hill's *VulnToolKit* R package, designed for the analysis and summary of tidal datasets. *VulnToolKit* includes functions to identify tidal cycles, calculate the proportion of time Inundated at a given elevation, and find the median length of time inundated at a particular elevation.

One of the objectives for using this water logger array sampling protocol was to be able to produce for each site, a predictive model for where flooding would occur not just at the locations of the water loggers but for any location within the salt marsh site. We want this model so that we can verify or at least compare it to the water detection capabilities of the aerial imagery. To extrapolate beyond the locations of water loggers to other locations within a salt marsh, we expected that we would need to develop a predictive model that does not simply rely on elevation data. We expect that we will need to account for the other factors that might delay or facilitate flooding, or prevent flooding or drainage for any particular location.

Thus far, we have done an initial analysis for the Red River site, with plans to perform this analysis at all of our sites. In order to assess the relationship between elevation and Proportion of Time Inundated, and elevation and Median Duration of Inundation, we removed outlier loggers that either report no inundation or near constant inundation throughout the logger deployment period. The loggers that report near constant inundation were mostly located in ponds, which do not experience the same degree of water fluctuations as platform or creek loggers.

Our primary approach thus far has been a statistical method where we first take elevation data for all water logger locations (recorded using a Trimble RTK GPS unit) and correlate those data with three inundation metrics derived from water logger data: 1) Depth of Inundation, 2) Median Duration of Inundation, and 3) Proportion of Time Inundated. Two of these metrics were used as response variables for the initial regression.

Proportion of Time Inundated: This metric quantifies the proportion of time that a logger is inundated by water. We calculated this metric by classifying 10-minute time intervals as either flooded or not flooded and divided the number of flooded intervals by the total number of intervals. This metric represents the proportion of time a location was inundated during the entire time the logger was deployed, generally 2-3 weeks.

Median Duration of Inundation: This metric is based on the length of time a water logger at a given location was flooded per inundation event. We calculated the metric by classifying groups of time intervals as inundation events, summing the time intervals for each event, and then finding the median length of time from among all inundation events (reported as hours or fractions thereof) that occurred during the period when loggers were deployed.

In our initial regressions between elevation and Proportion of Time Inundated, and elevation and Median Duration of Inundation, we see a strong negative relationship between elevation and both hydrology metrics (Figure 19 and Figure 20). Our next step will be to regress the residuals against secondary variables and evaluate whether secondary variables associated with water movement, such as flow distance to the nearest channel and flow distance to ocean, can account for unexplained variation in the hydrology metrics. We intend to use elevation, plus any secondary metrics that were significant in explaining residual variation, to construct a model of how water moves across the marsh for each of our study sites.

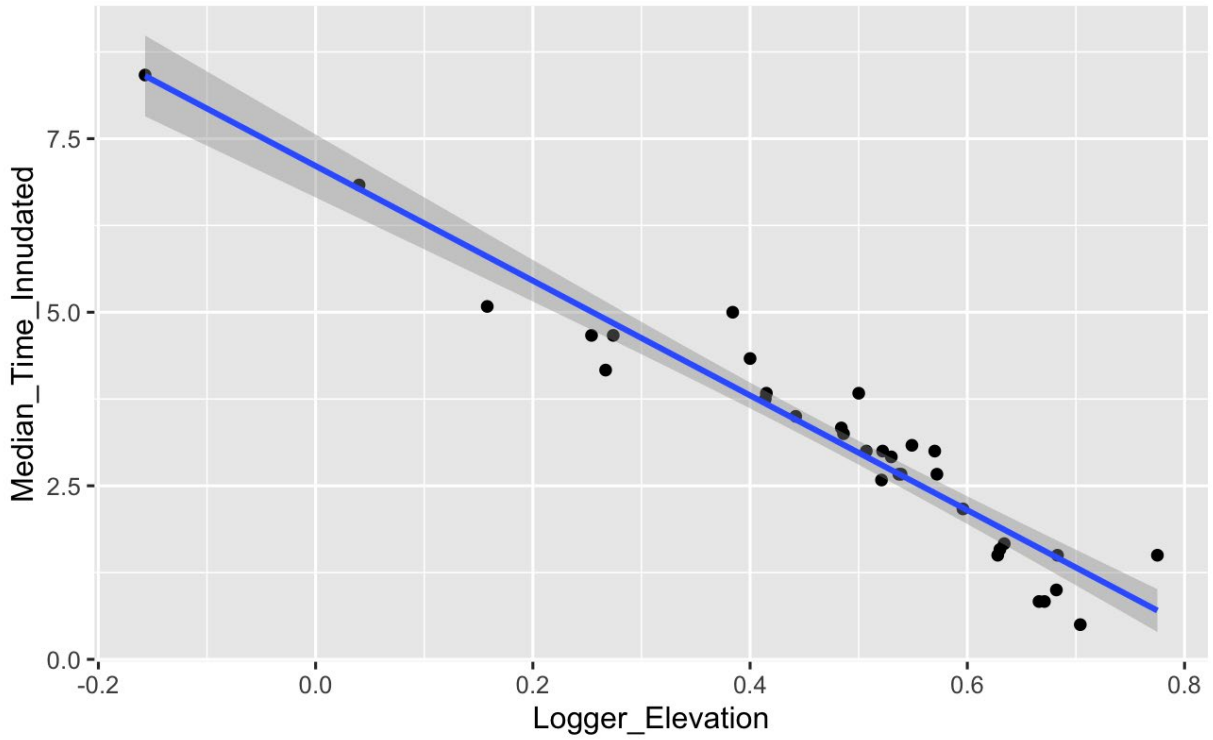

Figure 19 - Median Duration of Inundation for discrete flooding events recorded by a given logger vs. the elevation of that logger

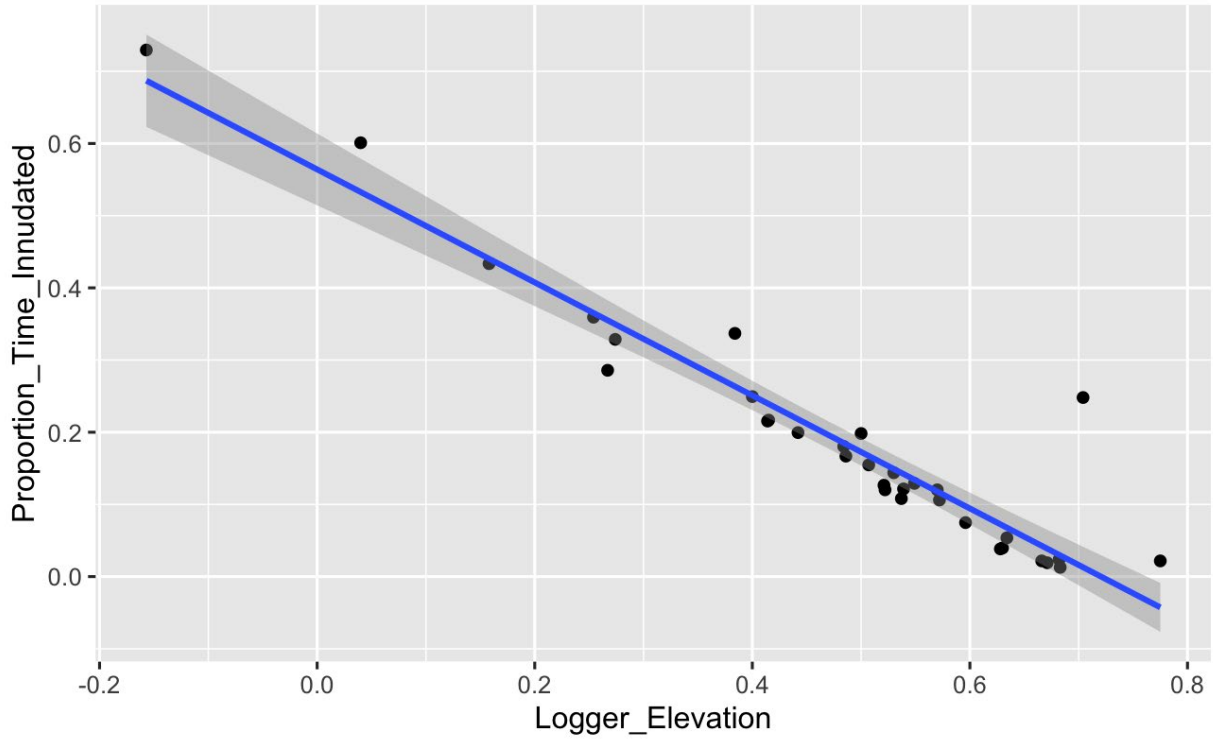

Figure 20 - Portion of time a given logger was inundated over the course of its deployment vs. the elevation of that logger

A digital terrain model (DTM) produced with filtered LiDAR data collected by UAS (Figure 21, described further in the next section) was used to model the routing path of water flowing through the Red River salt marsh during a typical tide cycle (Figure 22 and Figure 23). We believe that these paths and networks are likely to play an important role in determining where and when different portions of the marsh are inundated. We are still exploring variables that might have significant explanatory power for our hydrology metrics. Once we identify significant variables, we will produce a model for predicting inundation patterns for all locations within the marsh. We intend to compare the results of this model to the inundation patterns estimated by an analysis of spectral indices from NIR and SWIR imagery to determine which method is more accurate. In a future phase of the research, we intend to collect additional water logger data at our study sites to more rigorously test the accuracy of both approaches.

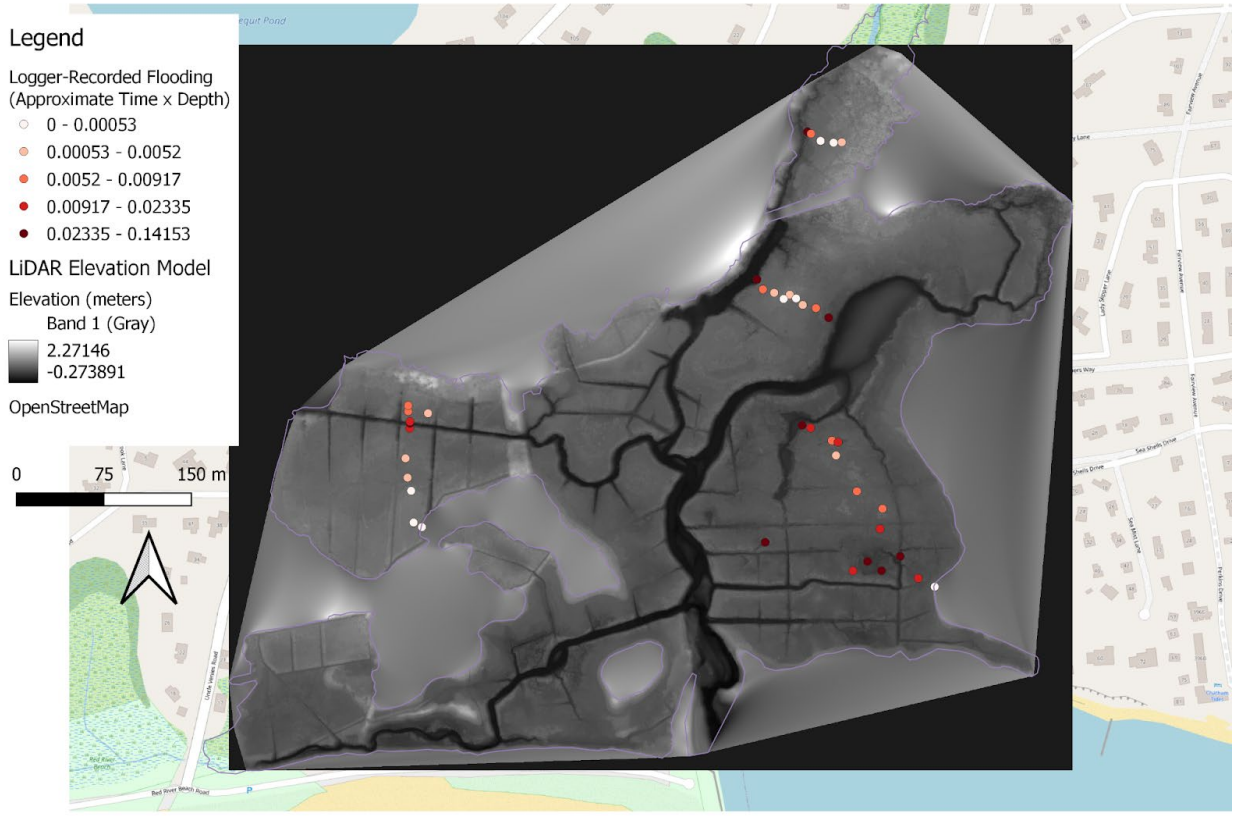

Figure 21 - Water logger locations at the Red River site mapped to a DTM derived from Hesai XT32 LiDAR after filtering to exclude vegetation cover

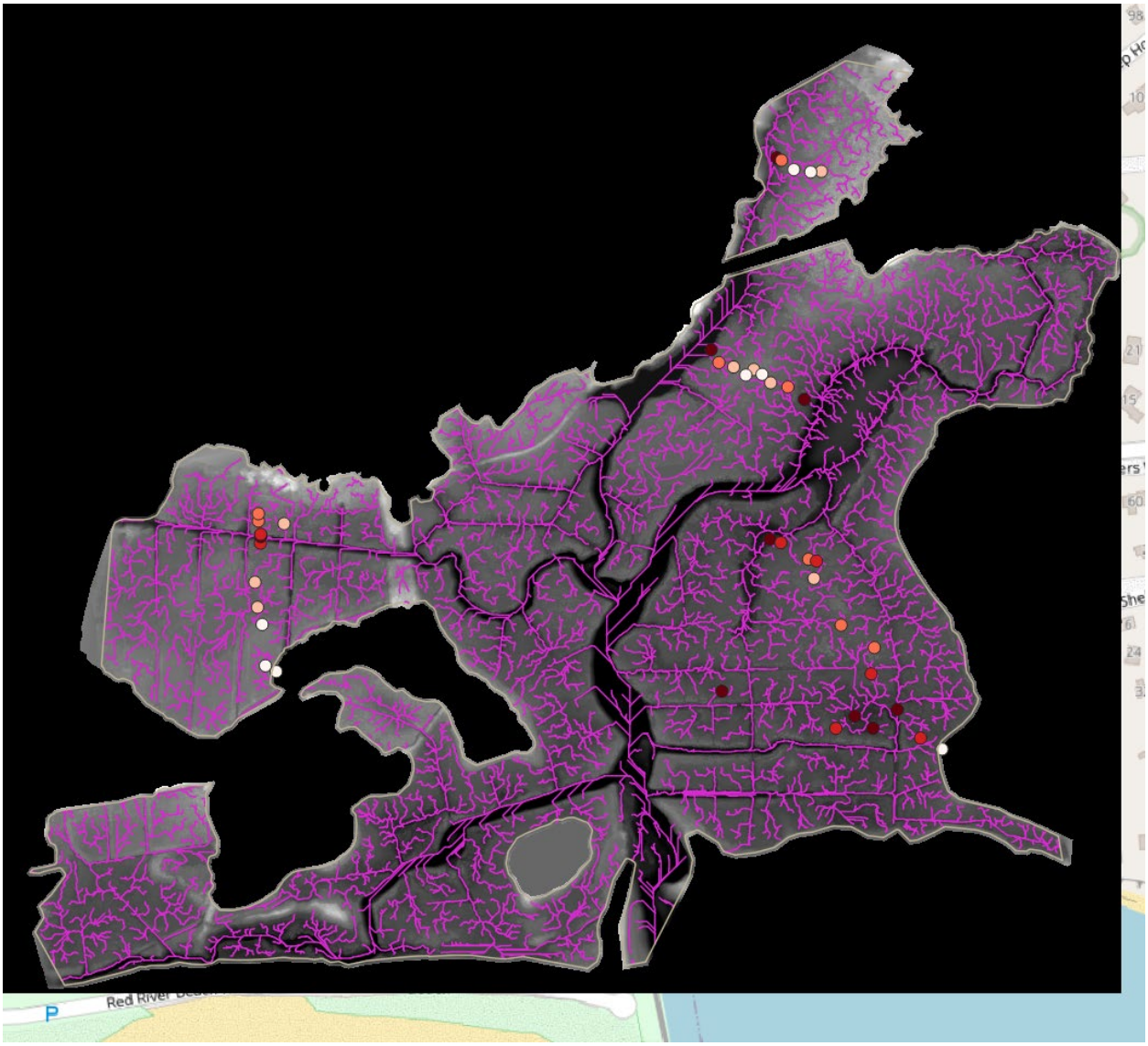

Figure 22 - Flood routing paths at the Red River site (shown in magenta) as derived from the DTM

Figure 23 - Flood routing pathways of Strahler Order 5 or greater are shown in a thicker red line. Euclidean distance and flood pathing to these higher-order paths could potentially be a significant explanatory variable for predicting inundation metrics.

Identification of embankments and assessment of impacts

Purpose

Our objective for this component of the research was to assess the accuracy of UAV-mounted LiDAR compared to the UAV-based RGB photogrammetry that had previously been used to produce all of our DEMs. Improvements in sensor design, along with their integration into “plug and play” LiDAR remote sensing payloads, have made LiDAR technology increasingly accessible for research. The newly introduced Remote Sensing Payload Instrument (RESEPI) produced by Inertial Labs was acquired by the UMass Amherst College of Engineering in early 2022 and was lent to our team shortly thereafter. Tests were carried out with the device in early spring, and the first implementation flight at Old Town Hill took place in May of 2022.

LiDAR and Creation of DTMs

In the 2022 field season, flights were conducted with UAV-mounted LiDAR at three of our study sites. At each of the three sites (Old Town Hill, Red River, and Wellfleet Bay), two flight campaigns were carried out: one early in the growth season, when plant biomass was at its seasonal low, and another during the peak growth season when vegetation had reached its maximum mature height. An additional early season flight was carried out at the Horseneck Beach site; however, no peak season flight was conducted at that site because it was not a site selected for the embankment research (discussed below).

All flights used the RESEPI, with its integrated Hesai XT-32 LiDAR unit and ADTi 24MP camera, mounted in a nadir position onto the DJI Matrice 600 (Figure 24). Except for the convergence maneuvers required for static and kinematic alignment, all surveyed flight plans were flown autonomously with DJI’s Ground Station Pro (GS Pro) application. Flight transects were flown in a continuous boustrophedonic pattern. Transect altitude and side overlap were chosen specifically to produce point clouds.

Figure 24 - RESEPI with its integrated Hesai XT-32 LiDAR unit, and the unit mounted to the DJI Matrice 600

Table 7 - Dates of LiDAR flight campaigns for each of four sites

Site	Early Season	Peak Season
Old Town Hill	14 May 2022	11 August 2022
Wellfleet Bay	20 May 2022	2 August 2022
Red River	26 May 2022	10 August 2022
Horseneck Beach	20 May 2022	N/A

All LiDAR point clouds were created in PCMaster, a proprietary software provided by Inertial Labs. The RESEPI has an onboard Real-Time Kinematic (RTK) and Post-Processed Kinematic (PPK) global navigation satellite system (GNSS) that negates the need for GCPs. For the PPK workflow used by this project, Receiver Independent Exchange Format (RINEX) data were acquired from the Massachusetts Continuously Operating Reference Station Network (MaCORS). PCMaster used this to process the forward and reverse trajectory, producing an accurate post-processed trajectory. Other steps undertaken in PCMaster included initial filtering to remove stray points and inaccuracies caused by low scan angles. An additional software, LASTools by Rapidlasso GmbH, was used for a datum transformation and to clip the flight area to the desired bounds. All point clouds constructed using RGB photogrammetry were created in Agisoft Metashape following our standard protocol (as outlined in the QAPP).

Multi-return LiDAR's success at penetrating vegetation canopies does not apply to the dense ground vegetation of the salt marsh. While some returns may penetrate the grass canopy, most returns are from the canopy of the vegetation or from somewhere between the canopy and the ground surface (Curcio et al., 2022; Hladik & Alber, 2012). This necessitated the use of filtering to produce a model that more accurately represented the peat surface. "Ground points" and "Non-ground points" were classified using the Cloth Simulation Filtering (CSF) tool in the open source software CloudCompare. Three rounds of CSF processing (Table 8) were required to achieve the desired results. When analyzed, some models that had been processed three times were over-filtered, meaning two rounds of processing produced the best results (smallest RMSEs and largest R^2 values). In ArcGIS Pro (ESRI), the classified "Ground points" were thinned and then rasterized to produce the final DTM product. "Non-ground points" can be rasterized without further filtering to produce CHMs.

Table 8 - Cloth Simulation Filtering (CSF) processing parameters for each "round" of processing. Cloth resolution and classification threshold are doubled for each round of processing.

Round of Processing	Cloth Resolution (m)	Max Iterations	Classification Threshold (m)
1	0.05	500	0.03
2	0.10	500	0.06
3	0.20	500	0.12

The DTMs were analyzed using a series of RTK measurements taken on the marsh platform from the 2020 to 2023 field seasons. 491, 538, and 311 RTK measurements were taken at Old Town Hill, Red River, and Wellfleet Bay, respectively. RTK measurements were dispersed throughout the site footprint and were only located in areas of the marsh platform above water at low tide (Figure 25). While some measurements were taken in vegetation up to 300 cm tall (e.g., *P. Australis*), most were taken in grasses that grow about 30cm high (e.g., *S. Patens, S. Alterniflora* - short form).

The difference between each RTK ground measurement and the corresponding DTM measurement was calculated. Then, the RMSE (Root Mean Square Error) was calculated with each set of residuals (Table 9 and Table 10). Filtered LiDAR showed improvements over the RGB photogrammetry. Early season flights offer an advantage due to the senesced vegetation.

Table 9 - May 2022 LiDAR RMSE (m) with CSF filtering and thinning. Two Rounds of CSF Filtering produced the best results at Old Town Hill and Red River. Three rounds of CSF filtering produced the best results for Wellfleet Bay. Gray-shaded cells represent best results. Unfiltered RGB RMSE measurements are listed for comparison.

Site	**May 2022 LiDAR Two Rounds of CSF Filtering**	**May 2022 LiDAR Three Rounds of CSF Filtering**	**May 2022 RGB photogrammetry**
Old Town Hill	0.144	0.190	0.627
Red River	0.107	0.108	0.431
Wellfleet	0.119	0.116	0.214

Table 10 - August 2022 LiDAR RMSE (m) with CSF filtering and thinning. Two Rounds of CSF Filtering produced the best results at Old Town Hill and three Rounds of CSF Filtering produced the best results at Red River and Wellfleet Bay. Gray-shaded cells represent best results. Unfiltered RGB RMSE measurements are listed for comparison.

Site	Aug 2022 LiDAR Two Rounds of CSF Filtering	Aug 2022 LiDAR Three Rounds of CSF Filtering	Aug 2022 RGB photogrammetry
Old Town Hill	0.154	0.184	0.829
Red River	0.143	0.134	0.485
Wellfleet Bay	0.198	0.179	0.500

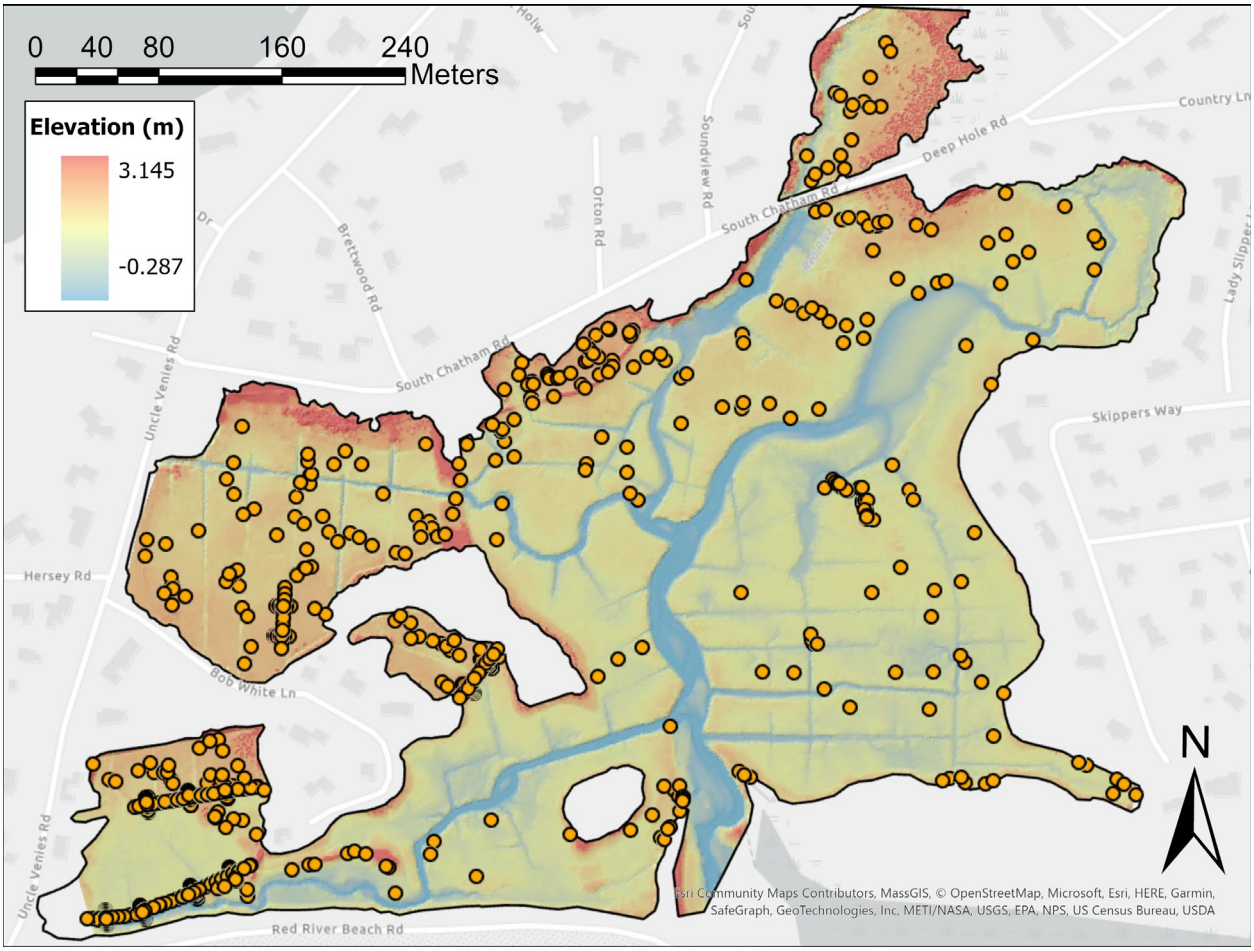

Figure 25 - Red River LiDAR DTM with survey points

Identification of Embankments

Embankments or dykes are a common anthropogenic feature found at a number of our study sites. Many of these structures were constructed in the 19th century or earlier for agricultural purposes and have since been abandoned, while others remain highly utilized, such as those supporting modern roadways. These extant embankments, both utilized and abandoned, have significantly altered the topography of salt marshes, resulting in numerous geophysical and ecological responses.

The ease of finding these structures varies, with maintained roadways being simple to find, but small-scale agricultural berms being almost imperceptible. With the high accuracy DTMs produced from UAV-mounted LiDAR, we have been able to identify and map many of these structures at two of our study sites: Old Town Hill and Red River (Figure 26). Some mapped embankments were delineated using survey points taken at regular intervals with the Trimble R10 RTK (Figure 27).

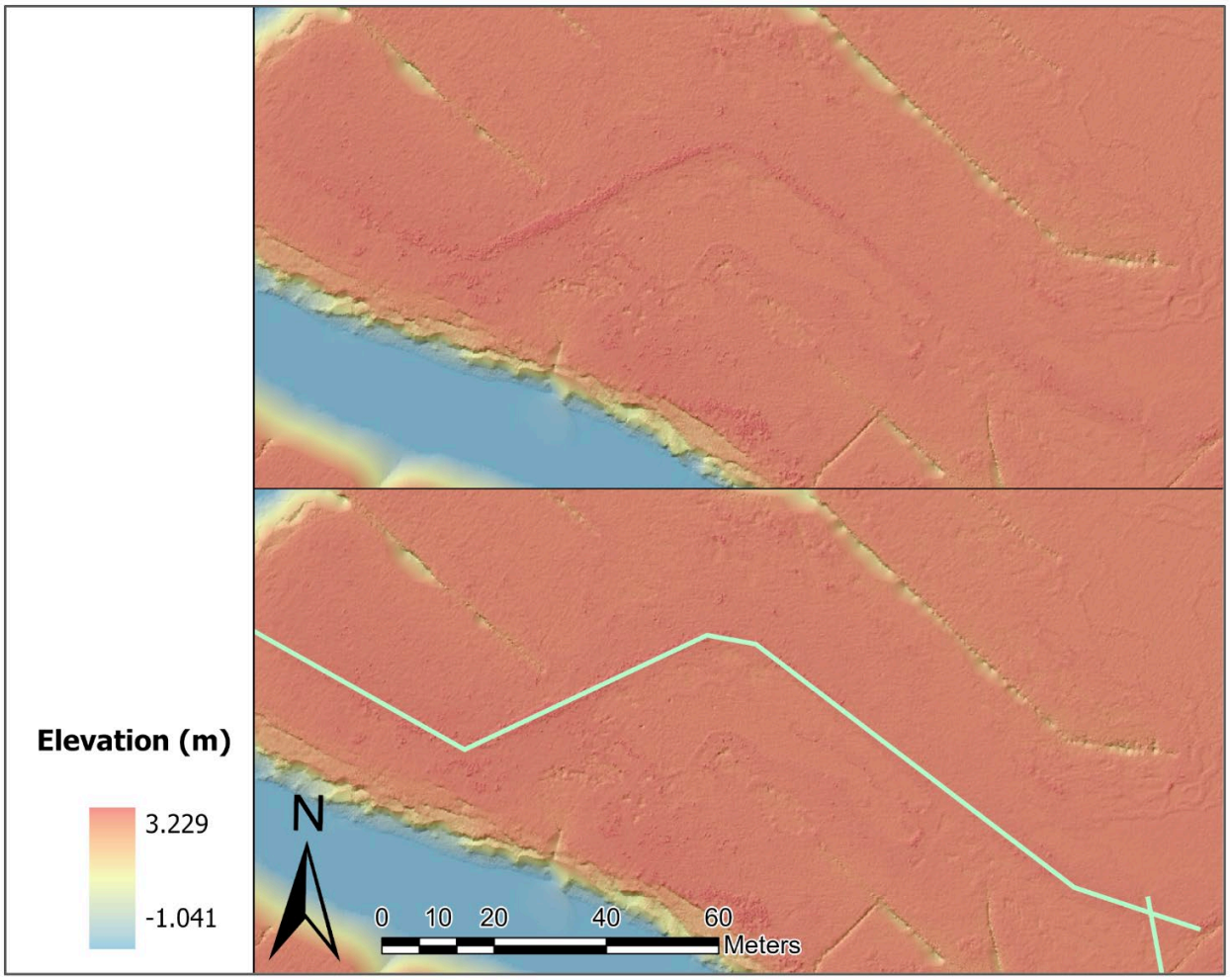

Figure 26 - Delineating an embankment with LiDAR at Old Town Hill

Figure 27 - Surveying a low agricultural embankment previously delineated with LiDAR at Red River

We are now actively conducting analyses using multispectral orthomosaics and our classification models to assess the impact these embankments are having on salt marsh topography, hydrology, and vegetation. For example, Figure 28 illustrates a scenario, where a spring high tide NIR image reveals how an agricultural embankment has altered platform flooding patterns.

Discussion and Lessons Learned

Our work with LiDAR has shown that it offers several benefits over other methods for producing DTMs. LiDAR flights are relatively simple to conduct and require less image flight overlap than conventional photogrammetry, meaning flight times are reduced. Additionally, the presence of an onboard RTK/PPK negates the need for the installation and location of GCPs, a normally time consuming and laborious process in disjointed landscapes such as salt marshes. The lack of GCPs also greatly reduces processing time, as the GCP tagging processes are also time consuming. Generating an initial point cloud with data captured on the RESEPI is a straightforward process that requires a fair amount of computer processing time, but minimal human input.

The key benefits of working with LiDAR are the output model results. RMSEs of DTMs produced with LiDAR showed significant improvements over those produced with RGB photogrammetry. Further, the LiDAR DTMs produced much larger R^2 values (0.693 to 0.914) indicating the models provided a good fit to the RTK points surveyed.

Figure 28 - High spring tide NIR imagery at Red River. This high embankment (delineated in blue) has reduced flooding in areas of the platform to the northwest of it. Areas of inundation appear darker in NIR imagery.

Cloth Simulation Filtering (CSF) was an effective method of classifying "ground points" and "non-ground points," an essential step in producing an accurate DTM. Although it was designed to be user friendly, utilizing the CSF filter proved to be more challenging than anticipated. While the fine cloth resolution and classification threshold were chosen with the size and spacing of salt marsh vegetation in mind, in practice we were highly limited by the available system memory capacity of our remote desktop. The CSF filter is memory intensive and it was not uncommon for filtering processes to max out our remote desktop's 128 GB installed memory. The first round of processing took anywhere from twelve to forty-eight hours to process and could abnormally end at any time due to an out-of-memory error. This meant that processing our seven LiDAR models through the CSF filter took much longer than was anticipated. Increasing the cloth resolution and classification threshold could have prevented this error but would not have produced the results we sought to achieve.

While our current methods have provided valuable insights into the accuracy and efficiency of data acquisition, there is room for improvement and optimization. Opportunities for improvement range from data collection procedures to data filtering. Higher overlap to allow for a further reduction of scan angles could enable more LiDAR returns to capture the peat surface. The refinement of filtering algorithms, whether that be with CSF or some other tool, could yield improved DTM results. Investigating strategies such as these could yield better results with the LiDAR and UAS technology that we currently have available.

Identification and Mapping of Eroding Creek Banks

Figure 29 - Slumping bank. Portions of the channel bank are separating from the marsh platform and sliding into the channel

Purpose

Eroding creek banks (Figure 29) are one indicator of a declining marsh (FitzGerald & Hughes, 2019). Using drone imagery, the objective of this component of our project is to use image analysis techniques from machine learning to identify sections of eroding banks. If successful, a quantitative measure can be obtained for an entire marsh. This component was not in our original scope of work but was added when an opportunity to collaborate with computer scientists at the University of Oregon presented itself.

Using a machine learning approach requires feeding a model a set of images as training data, images that contain both positive and negative examples of erosion. Typically, the number of images necessary can be large. This can be a bottleneck given a human must painstakingly go through perhaps thousands of images and label each as positive and negative. A secondary goal of the project is to avoid this bottleneck by using new machine-learning techniques that require much smaller sets of training images to obtain equivalent (good) results.

Object Identification

Our approach is to divide a large orthomosaic image produced from drone overflights of a marsh into smaller tiles. The size of these tiles required exploration by the team. Ultimately, we chose a final value of eighty-one square meters (9m x 9m) for the tile size for the Old Town Hill site, sixty-four square meters (8m x 8m) for the Essex Bay and Peggotty Beach sites. The variation in tile size among sites was the result of variation in the resolution of orthomosaics produced for each site, and sizes were adjusted to achieve tiles that were 299 pixels x 299 pixels. These tile sizes offered enough ground coverage to differentiate intact banks from eroding banks. Larger tiles tended to mix positive and negative into one tile. Smaller tiles tended to identify one self-contained portion of a bank into what appeared as separate portions.

Training images were drawn from these tiles and labeled as positive (eroding) or negative (intact). Because this is a human-centric process, the team explored means to mitigate this labeling process. The outcome was to choose a relatively new machine learning technique called transfer learning. The general idea is to use a pre-trained model as a starting point. A surprising aspect of this approach is that the pre-trained model is trained on images that often have nothing to do with salt marshes or even natural landscapes. Results from the pre-trained model were transferred to a different domain with a relatively modest number of new training data from that domain to build a new model linked to the bank erosion problem. We chose Google's Inception model as the transfer learning component. We then created a separate backend for Inception that finished the process of producing positive and negative classifications of eroding banks. Using this combination, we were able to drastically reduce the number of tiles that a human had to hand-label.

Object Classification

We choose three different sites (Old Town Hill, Essex Bay, and Wellfleet Bay), each with its own unique characteristics of bank erosion. Training data from each of the three sites were used for the classification model. Data were limited to drone images taken early to late spring during low tides. We chose to use three classes: positive (bank erosion), negative (intact bank), other (marsh platform).

Example Images

Figure 30 is a tiled image taken from one of our training sites, Old Town Hill. The green colored tiles are ones that have been classified as positive (eroding bank). This approach showed mixed results. The tiles along the creek banks are accurately predicted. However, there are also tiles on the marsh platform that are misclassified as eroding banks. We speculate that this can be cleaned up by a pre-processing masking step that masks out most of the platform, limiting the classification to channel banks. The next image (Figure 31) is from a different site, Essex Bay. The tiles colored purple are classified as negative (clean banks). The model had fewer problems with misclassification of platform tiles for this site.

One of the problems we had with both sites was the model's honing in on the banks of ditches as well as creeks. In general, we do not see the state of ditch banks as contributing significantly to an assessment of salt marsh health. Masking out ditches by hand is a laborious process. We are considering one of two alternatives: (1) build a separate model that can identify ditches, and from that, automatically mask them out, or (2) add a 4th class to our model, ditch bank, with associated new training images. This class, along with the marsh platform class, could then be ignored. We are currently experimenting with both approaches.

Figure 30 - Tiled image of the Old Town Hill site. Green tiles are ones that have been classified as positive (eroding bank)

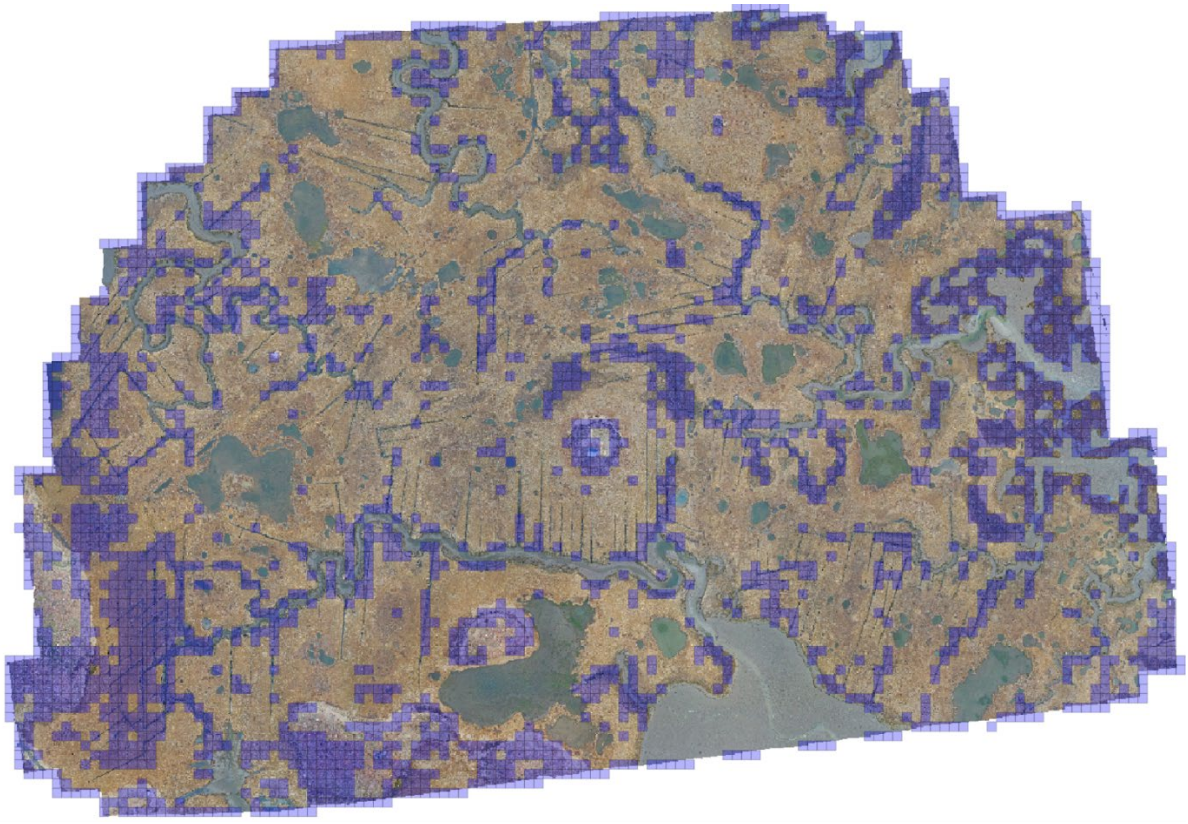

Figure 31 - Tiled image of the Essex Bay site. The purple tiles are classified as negative (intact banks)

Accuracy

Using the traditional approach to evaluate a model, we divided the tiles we hand-labeled into a training set and a test set. Our accuracy on the test set was 99% across the three different sites we sampled. This result was from a single model trained from and applied to all three sites (with their different peculiarities) as opposed to three separate models, one for each site. This shows promise for a single model with general classification power across a wide range of marsh sites. The overall accuracy of our model is likely to be overstated because the 99% accuracy was based on a validation test that only considered tiles of channel banks. The accuracy will undoubtedly be lower when including marsh platform tiles.

We also did an informal spot-check of the tiled images from the various sites that were not included in our training or test sets (see Figure 30 and Figure 31, where we applied the trained model to entire sites). We were encouraged by these results and used them to further refine our training and test sets. We expect this cycle of model training, tile classification, spot-check, model retraining will lead to increasing accuracy.

Future work

We will continue working with different approaches for using object identification and classification, with the objective of automating the identification and mapping of eroding channel banks. So far, this work has used only the visible RGB bands from our remote sensing imagery. We plan to investigate the inclusion of NIR data to focus the model more exclusively on channel banks. From this work, it should be possible to create a bank erosion metric that can be applied across each study site.

The spectral data we are using is of very high resolution (between 2.7cm and 8.3 cm, depending on the particular camera system used for data capture), which may limit its usefulness to sites where these UAS data have been collected. However, aerial photogrammetry data available statewide from the Massachusetts Bureau of Geographic Information (MassGIS) is also of high resolution (15 cm), contains RGB and NIR bands, and was flown under spring “leaf off” conditions. One aspect that it does not provide is the ability to focus analyses on specific stages in the tide cycle (low tide, mid tide, high tide). Assuming that we are successful in creating a channel bank erosion metric using our UAS-collected data, we plan to investigate the potential of creating a statewide metric using the state’s imagery. This new condition metric (bank erosion) could then be included in the CAPS model of ecological integrity for salt marshes, statewide.

Effects of ribbed mussels on salt marsh surface elevation

Purpose

A recent paper published in Nature Communications by Crotty et al., (2023) describes the ecological engineering capability of *Geukensia demissa*, the Atlantic ribbed mussel. Mussels are filter feeders; they process large amounts of water and deposit feces and pseudofeces, adding sediment to their surroundings. Crotty et al., through a series of creekshed-scale experiments found that mussels are driving greater marsh accretion in the areas where they are more densely populated. This study, conducted in the Chesapeake Bay region, prompted our research team to undertake an exploratory study at one of our salt marsh study sites. We set out to sample the mussel population and see if any relationship was evident between local elevation and mussel density. This preliminary study was an undergraduate summer student project funded by the UMass Center for Agriculture, Food, and the Environment that utilized our LiDAR and NIR images at one of our sites, as well as original field research involving the counting of mussels.

Methods

We selected Wellfleet Bay as our study site as it features substantial vegetative dieback and exposed substrate on the marsh platform facilitating an accurate mussel count. To conduct our mussel count we used a 1-meter x 1-meter quadrat along six transects, approximately parallel to a channel bank (Figure 32). At each of the corners of quadrat the Trimble Real Time Kinematic (RTK), was used to record precise coordinates and elevation (Figure 33). A team member counted the mussels in each quadrat.

In data processing, we overlaid a LiDAR layer from 2023 with the plotted quadrats and found the mean elevation of the quadrat. Next, we analyzed mussel counts compared to mean elevation of each quadrat, separating the quadrats by transect and analyzing each transect as one dataset. In a separate analysis, we overlaid two NIR orthomosaics, high tide and low tide from the same day, to compare the extent of the inundation. We compared the difference in color saturation between the high and low tide for each quadrat, with higher numbers indicating more inundation. Then we conducted an analysis of mussel counts and inundation extent.

Results and Discussion

This exploratory study did not demonstrate an obvious relationship between mussel density and elevation or tidal inundation (Figure 34). Some transects, such as three and five, showed a positive relationship between mussel density and elevation, however the trend was not widespread nor consistent enough to justify conclusions about a link between mussel density and elevation. A larger experiment, such as the type conducted by Crotty et al., might provide more insight into these potential relationships. This exploratory study is an example of how the UAS Salt Marsh project's vast collection of drone imagery and orthomosaics creates new analytic opportunities to understand salt marsh dynamics. It combined LiDAR and NIR images with original ground-based fieldwork. Remote sensing datasets have powerful capabilities for future researchers to gain deeper insights into tidal marshes.

Figure 32 - Counting mussels in a 1 meter x 1 meter quadrat placed close to a denuded bank

Figure 33 - Recording the elevation and precise location of a quadrat using the Trimble RTK device

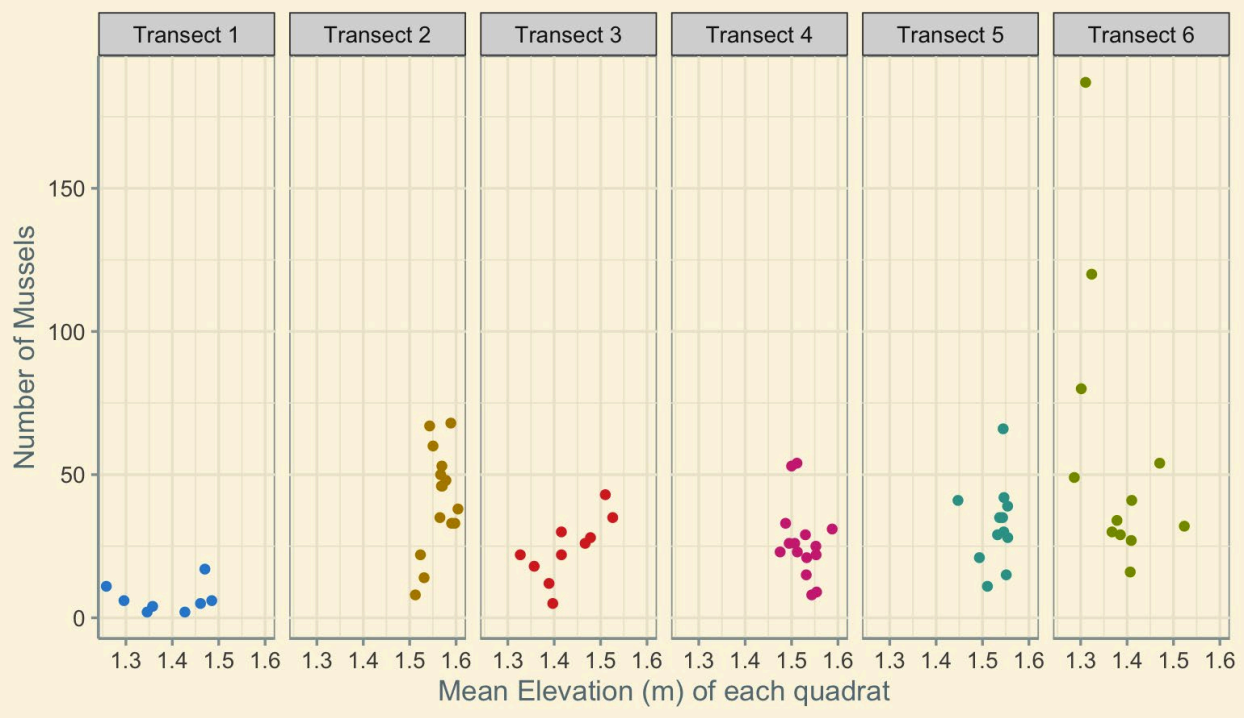

Figure 34 - Elevation and mussel counts by transect

Conclusion

Wetlands can be difficult places to conduct field research and for assessment and monitoring. Salt marshes, with their restricted access due to daily tides, abundant water features, and often-soft substrates, can be especially challenging for fieldwork. Remote sensing technologies offer the potential to avoid these challenges and generate data that can be used for salt marsh condition assessment and monitoring. However, traditional remote sensing data (aerial photography and satellite imagery), though widely available, may not be well timed to specific points in the tide cycle that may be needed to produce the most useful data. Remote sensing data collected by drones and sensors during specific phases of the tide cycle has the potential to overcome the difficulties of access confronting ground-based data collection and the timing issues that limit the usefulness of traditional remote sensing data.

Unoccupied Aerial Systems (drones and sensors) are a relatively new technology for environmental assessment and monitoring and applying UAS technology to salt marsh assessment and monitoring comes with its own challenges. Standardized UAS protocols for data collection, image processing and data analysis are not yet widely available. Reliability of equipment varies and the loss of vehicle availability due to crashes or routine wear and tear can limit data collection during relatively short field seasons. Multiple software programs are needed to process images and analyze UAS data, and these programs can be buggy. Further, working with large stacks of high-resolution, multi-spectral data requires high capacity computing that is not always easy to access.

Our research team has worked to overcome the challenges of UAS-based assessment and monitoring and has made significant progress. Complications associated with the Covid-19 pandemic and the temporary loss of high-capacity computing capacity slowed that work somewhat. However, we are close to finalizing protocols for using drones and sensors to produce detailed, high-resolution vegetation maps of salt marshes. Collection of hydrology data using arrays of water loggers allows us to link tidal hydrology to UAS images for our study sites. Complementary research is producing significant results on the use of LiDAR to produce reliable digital terrain models and in using those models to identify relic berms and embankments that are still affecting salt marshes today. Linking these DTMs to UAS spectral data allows us to assess the impact of these embankments on salt marsh hydrology.

It is our intention to continue this project for another two years in order to complete the work we have started and document open source protocols and procedures for others who wish to use UAS for salt marsh assessment and monitoring. Future work will focus on finalizing and integrating our primary data sets.

1. Land cover classification models
2. Elevation Models
3. Flooding and inundation models
4. Maps of spectral indices

Once we have reliable models for each of these categories, we intend to use parameters from these models to create metrics for salt marsh condition and vulnerability to sea level rise. We plan to leverage our large multi-temporal and multi-spectral stacks of orthomosaics from our study sites to investigate a cost-efficient, UAS-based data gathering strategy for understanding salt marsh condition and sea level rise vulnerability.

We believe that inundation patterns are likely to be closely correlated with elevation, and the two together can be used to define tidal hydrology throughout a salt marsh. We expect vegetation to reflect tidal hydrology, and hypothesize that categorical correlations between land cover and flooding patterns are indicative of a salt marsh's future viability. We believe that these patterns are detectable from vegetative form, phenology, or plant health indices measured with multispectral imagery, and that this approach can be used to create indices of salt marsh condition.

Our work using object identification and classification holds great promise for creating a bank erosion metric based on UAS data. We intend to explore the potential for using aerial imagery from MassGIS to adapt this metric for use throughout Massachusetts.

Condition or stressor metrics developed from this work will be integrated into CAPS models so that more accurate Index of Ecological Integrity (IEI) scores will be available for salt marshes statewide. As high-resolution aerial imagery becomes available in other states, these IEI models can be applied in other regions within the 13-states that make up the Northeastern U.S.

References Cited

Crotty, S. M., Pinton, D., Canestrelli, A., Fischman, H. S., Ortals, C., Dahl, N. R., Williams, S., Bouma, T. J., & Angelini, C. (2023). Faunal engineering stimulates landscape-scale accretion in southeastern US salt marshes. Nature Communications, 14(1). https://doi.org/10.1038/s41467-023-36444-w

Curcio, A. C., Peralta, G., Aranda, M., & Barbero, L. (2022). Evaluating the Performance of High Spatial Resolution UAV-Photogrammetry and UAV-LiDAR for Salt Marshes: The Cádiz Bay Study Case. Remote Sensing, 14(15), 3582. https://doi.org/10.3390/rs14153582

FitzGerald, D. M. and Z. Hughes. 2019. Marsh processes and their response to climate change and sea-level rise. Annu. Rev. Earth Planet. Sci. 2019. 47:481–517.

Hladik, C., & Alber, M. (2012). Accuracy assessment and correction of a LIDAR-derived salt marsh digital elevation model. *Remote Sensing of Environment*, *121*, 224–235. https://doi.org/10.1016/j.rse.2012.01.018

Jackson, S., A. Davis, K. Fickas, R. Wicks, J. Ward, and C Schweik. 2021. Developing methods for remote sensing of salt marsh condition using unoccupied aerial systems (UAS): Final report for EPA FY 2017-2018 Wetlands Program Development Grant CD 00A00312-3. University of Massachusetts, Amherst MA. 45 pp. (UMass-CD00A00312-3 Final Report.pdf)

Jackson, S. K. Fickas, C. Schweik, R. Wicks, A. Davis, and J. Ward. 2021. Quality Assurance Project Plan for Salt Marsh Research Using UAS and Remote Sensing as part of a Comprehensive State Monitoring and Assessment Program for Wetlands in Massachusetts: 2018-2023. EPA Grant Number (FAIN): 00A00312, RFA# 18095. University of Massachusetts, Amherst MA. 119 pp. (UMass Salt Marsh UAS-QAPP RFA# 18095_5-26-21.pdf)

Zhang, W., Qi, J., Wan, P., Wang, H., Xie, D., Wang, X. and Yan, G. (2016). An Easy-to-Use Airborne LiDAR Data Filtering Method Based on Cloth Simulation. Remote Sensing. 8(6), 501. https://doi.org/10.3390/rs8060501.

Appendix A – Salt Marsh Study Sites

We worked collaboratively with partners to collect data from nine salt marshes in Massachusetts from 2018 – 2023 (Figure 35). Sites along the North Shore of Massachusetts were Old Town Hill (Newbury) and Essex Bay (Essex). Sites along the South Shore were Peggotty Beach (Scituate), North River (Scituate), and South River (Marshfield). Sites on Cape Cod were Barnstable Great Marsh (Barnstable), Red River (Harwich and Chatham), and Wellfleet Bay Wildlife Sanctuary (Wellfleet). One site, Horseneck Beach (Westport), was on the coast of Buzzard's Bay. Each site had its own mix of hydrology, stressors, anthropogenic activities, and history of natural events. Below is a brief description for each of the nine salt marsh sites.

After we established an initial study area footprint for each site, it was decided to reduce the footprint size for several of the sites (to approximately 100 acres) to reduce the time required to fly the designated study areas. Reducing the time needed to acquire UAS imagery helped ensure that tide conditions did not significantly change between the beginning and end of each flight.

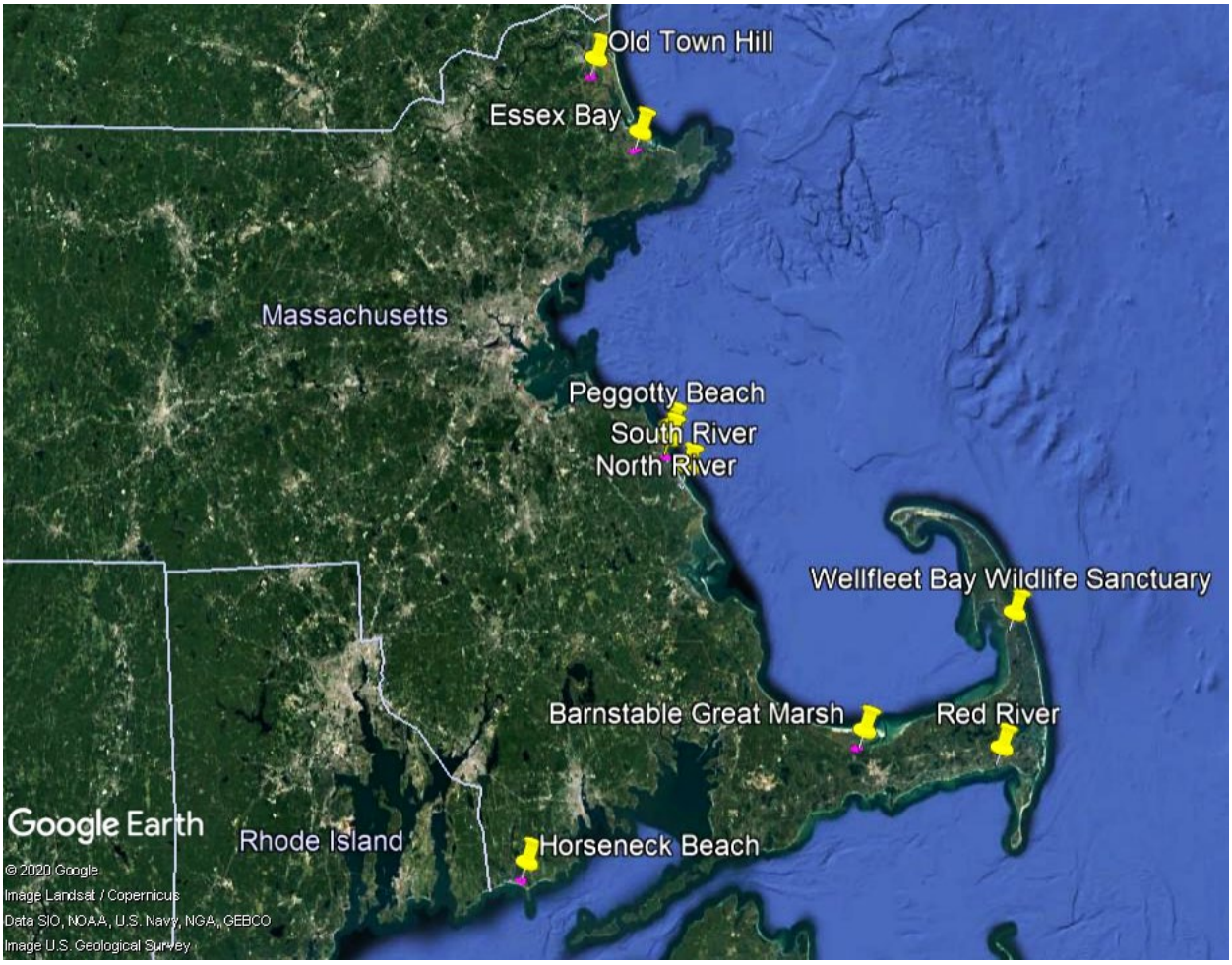

Figure 35 - Yellow pins identify the nine salt marsh sites that we assessed from 2018-2023 in Massachusetts

Old Town Hill

The Old Town Hill site (Figure 36) is located a few miles west of Plum Island and was selected because of specific interest expressed by The Trustees of Reservations (TTOR), which owns the land. TTOR has committed significant resources to studying a portion of the site, including developing a Sea Level Affecting Marshes Model (SLAMM) of land cover change over the next 50 years, which will complement the data that we collect. In 2020, TTOR began a salt marsh ditch remediation effort with an innovative nature-based method that was piloted at the U.S. Fish and Wildlife Service's Parker River National Wildlife Refuge. Walking trails are found throughout this site and it is a popular place for recreation and bird watching. Historically, this marsh was used to produce and harvest salt hay.

We installed 16 Ground Control Points (GCPs) (blue markers) at Old Town Hill that help us accurately georeference the imagery we collect so that they can be "stacked" and analyzed as a longitudinal dataset using geographic information systems (GIS) and other remote sensing analytic techniques. The full flight footprint covered 206 acres (outlined in blue) and had a perimeter of 3.8 miles. The reduced flight footprint covered 100 acres (outlined in bright pink) and had a perimeter of 2.26 miles.

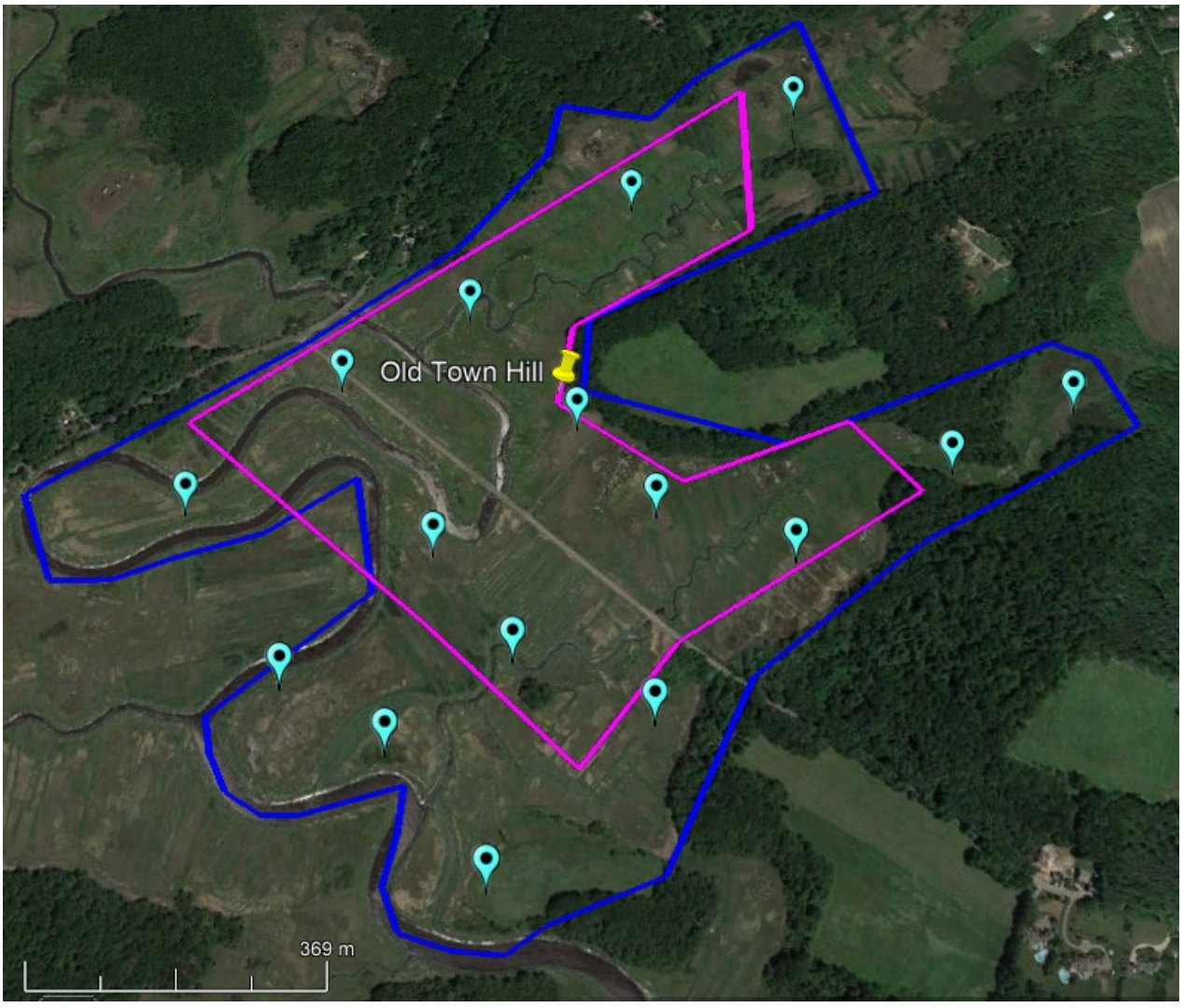

Figure 36 - Old Town Hill (Newbury, MA) - Partnered with The Trustees of Reservations

Essex Bay

The Essex Bay site (Figure 37) contains Dean's Island and is located behind the Cape Ann Golf Course. It was selected because of specific interest expressed by The Trustees of Reservations, which owns the land, and because it is a sentinel site being studied by MA Coastal Zone Management. During the winter of 2018, extreme cold, winds, and storm surge created notable sediment deposition events throughout the Great Marsh Estuary, which includes Essex Bay. A report about this event in Essex Bay has been published by Moore et al. 2019 from the University of New Hampshire.

We installed 14 GCPs (blue markers) throughout the Essex Bay study site. The full flight footprint covered 215 acres (outlined in blue) and had a perimeter of 2.3 miles. The reduced flight footprint covered 100 acres (outlined in bright pink) and had a perimeter of 1.53 miles.

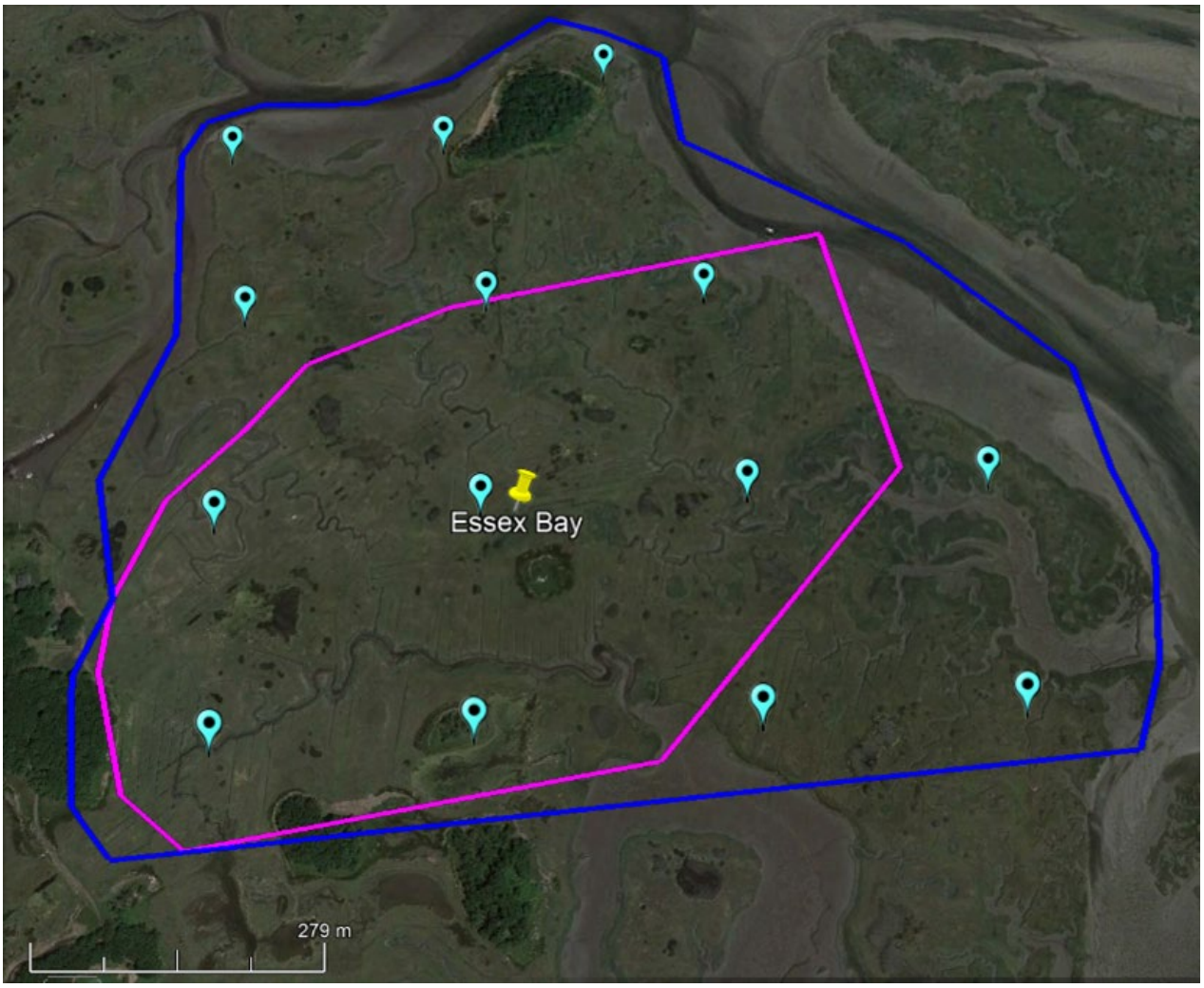

Figure 37 - Essex Bay (Essex, MA) - Partnered with The Trustees of Reservations and MA Coastal Zone Management

Peggotty Beach

The site at Peggotty Beach (Figure 38) is located in the town of Scituate. It was selected because an intensive study being conducted by a team of geologists from UMass Amherst will provide us with complementary date on sediment dynamics in this marsh. Nor'easters during the winter of 2018 drastically altered the beach and adjacent salt marsh morphology. This site presented an opportunity to study differences in spectral signatures associated with a rapidly changing salt marsh.

We installed 7 GCPs (blue markers) throughout the Peggotty Beach marsh. The full flight footprint covered 104 acres (outlined in bright pink) and had a perimeter of 1.88 miles. A reduced flight footprint was not needed for this site.

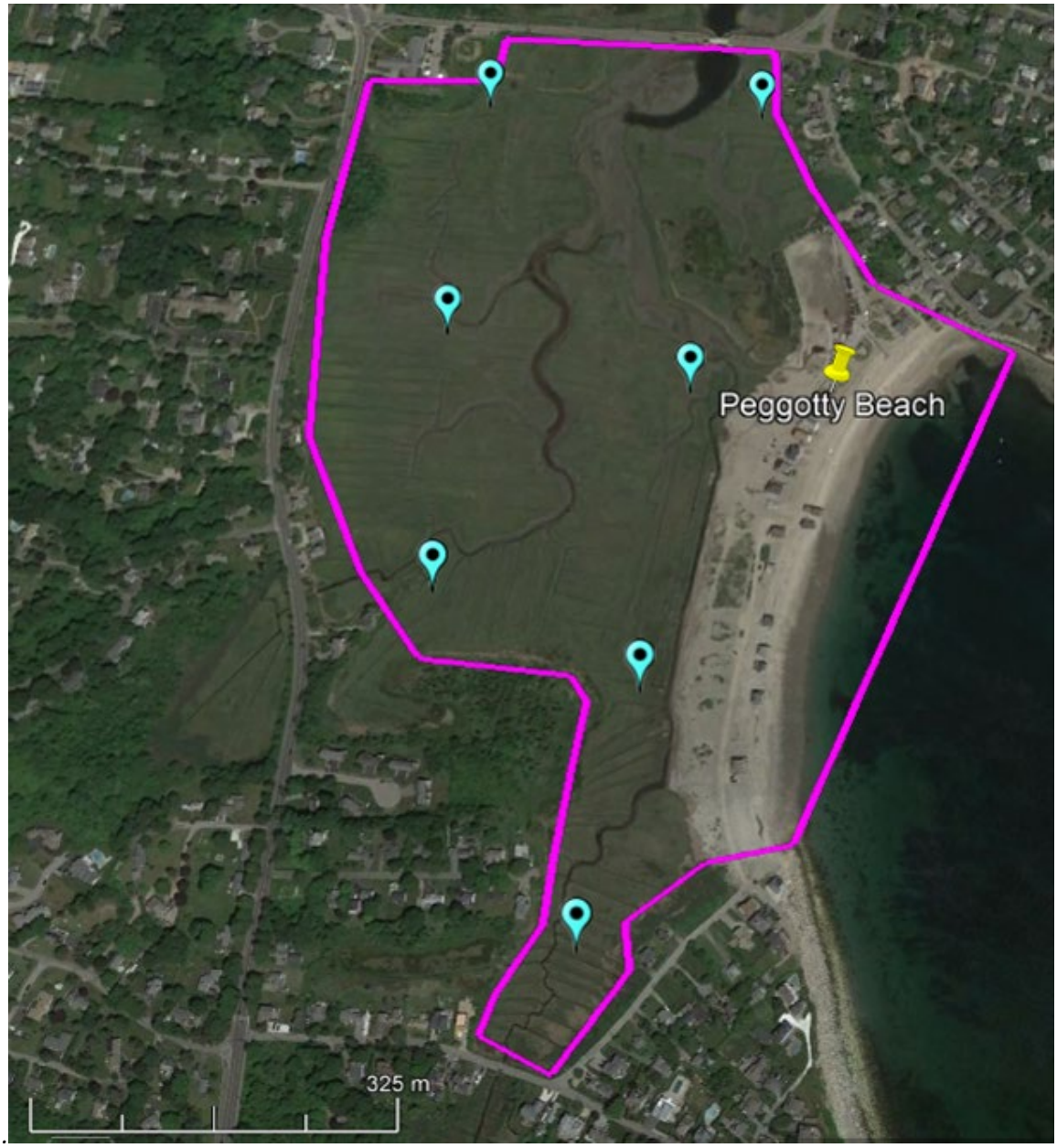

Figure 38 - Peggotty Beach (Scituate, MA) - Partnered with UMass Amherst Department of Earth, Geographic, and Climate Sciences

North River

The North River marsh site (Figure 39) is located at the mouth of the North River in the town of Scituate and contains portions of marsh owned by the Scituate Country Club. The beach area is overseen by the Massachusetts Audubon Society. This site was selected because 1) an intensive study being conducted by a team of geologists from UMass Amherst will provide complementary data on sediment dynamics, and 2) the opportunity to capture changes in beach morphology that is important to nesting birds.

We installed 9 GCPs (blue markers) throughout the North River inlet. The full flight footprint covered 163 acres (outlined in blue) and had a perimeter of 2.43 miles. A reduced flight footprint (outlined in bright pink) covered 90 acres and had a perimeter of 1.53 miles.

Figure 39 - North River Inlet (Scituate, MA) - Supported by Town of Scituate and Scituate Country Club; Partnered with UMass Amherst Department of Earth, Geographic, and Climate Sciences

South River

The South River marsh site (Figure 40) is located in the town of Marshfield, and it is currently being used for an intensive study of sediment dynamics being conducted by a team of geologists from UMass Amherst. We installed 11 GCPs (blue markers) throughout the South River inlet. The full flight footprint covered 144 acres (outlined in blue) and had a perimeter of 3 miles. A reduced flight footprint (outlined in bright pink) covered 97 acres and had a perimeter of 1.96 miles.

Figure 40 - South River Inlet (Marshfield, MA) - Supported by Town of Marshfield; Partnered with UMass Amherst Department of Earth, Geographic, and Climate Sciences

Horseneck Beach

The marsh site at Horseneck Beach (Figure 41) is located in the town of Westport and contains portions of a salt marsh managed by MA DCR. This site was selected because it is a sentinel site being studied by MA Coastal Zone Management and appeared to be experiencing subsidence and inundation issues. We installed 9 GCPs (blue markers) throughout the Horseneck Beach marsh. The full flight footprint covered 131 acres (outlined in blue) and had a perimeter of 1.76 miles. A reduced flight footprint (outlined in bright pink) covered 100 acres and had a perimeter of 1.6 miles.

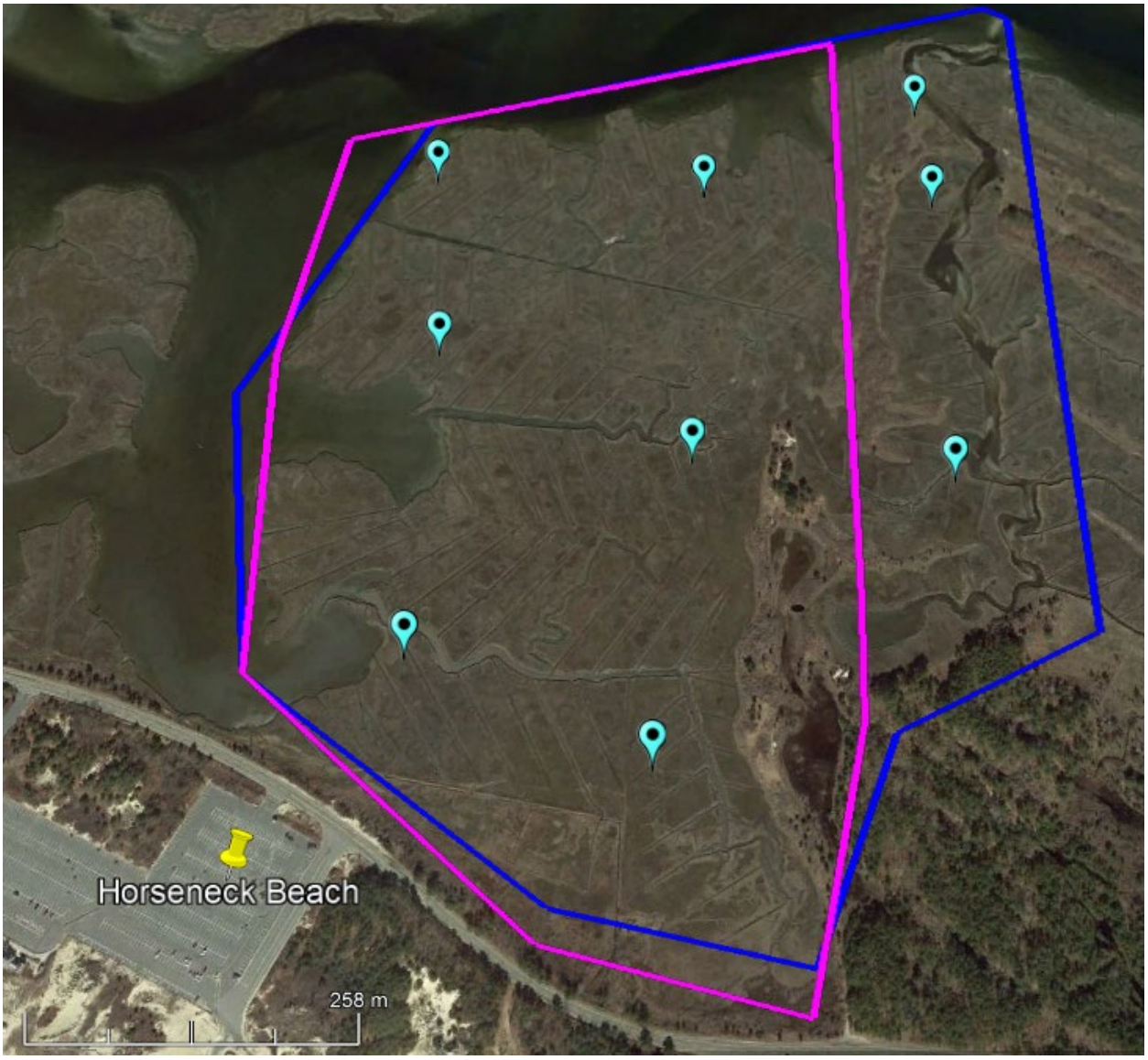

Figure 41 - Horseneck Beach (Westport, MA) - Supported by MA Coastal Zone Management and MA Department of Conservation and Recreation (DCR)

Barnstable Great Marsh

The new Barnstable Great Marsh study site (Figure 42), hereafter referred to as “Barnstable”, is located in the northwest portion of the Barnstable Great Marsh in the town of Barnstable and is managed as part of the Sandy Neck Beach Park. The boundaries of the study site were chosen to include both ditched and unaltered areas. We installed nine ground control points (GCPs) throughout the site. The flight footprint covers 40.5 hectares (100 acres) and has a perimeter of 2.91 km (1.8 miles).

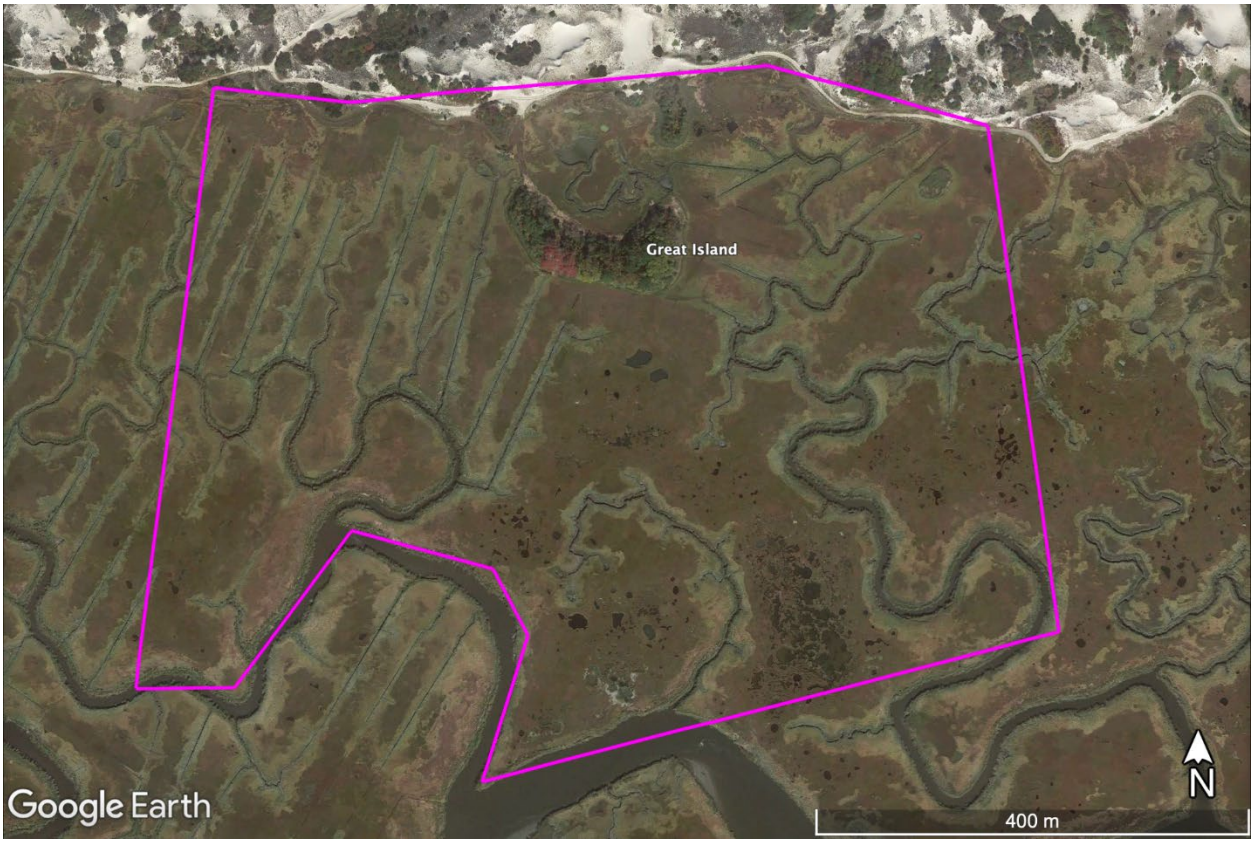

Figure 42 - Barnstable Great Marsh (Barnstable, MA) - Supported by the Town of Barnstable and the Sandy Neck Beach Park

Red River

The Red River marsh site (Figure 43) spans the Chatham and Harwich town line. It is managed by the Harwich Conservation Trust and the Chatham Conservation Commission. It was selected because of its proximity to a barrier beach, it contains a tidal restriction, has experienced restoration events, and appears to have interesting sediment dynamics. We installed 9 GCPs (blue markers) throughout the site. The full flight footprint covered 61.8 acres (outlined in blue) and had a perimeter of 2.43 miles. A reduced flight footprint (outlined in bright pink) covered 48 acres and had a perimeter of 2.15 miles. A reduced flight footprint was needed for this site to avoid flying over the cars entering the parking lot entrance.

Figure 43 - Red River (Chatham and Harwich, MA) - Supported by Harwich Conservation Trust and the Chatham Conservation Commission

Wellfleet Bay

The Wellfleet Bay Wildlife Sanctuary site (Figure 44) is located in the town of Wellfleet and is managed by the Massachusetts Audubon Society. This site was selected because it is a protected area that is experiencing extensive die back events and crab herbivory issues. We installed 10 GCPs (blue markers) throughout the Great Marsh. The full flight footprint covered 99 acres (outlined in bright pink) and had a perimeter of 1.83 miles. A reduced flight footprint was not needed for this area.

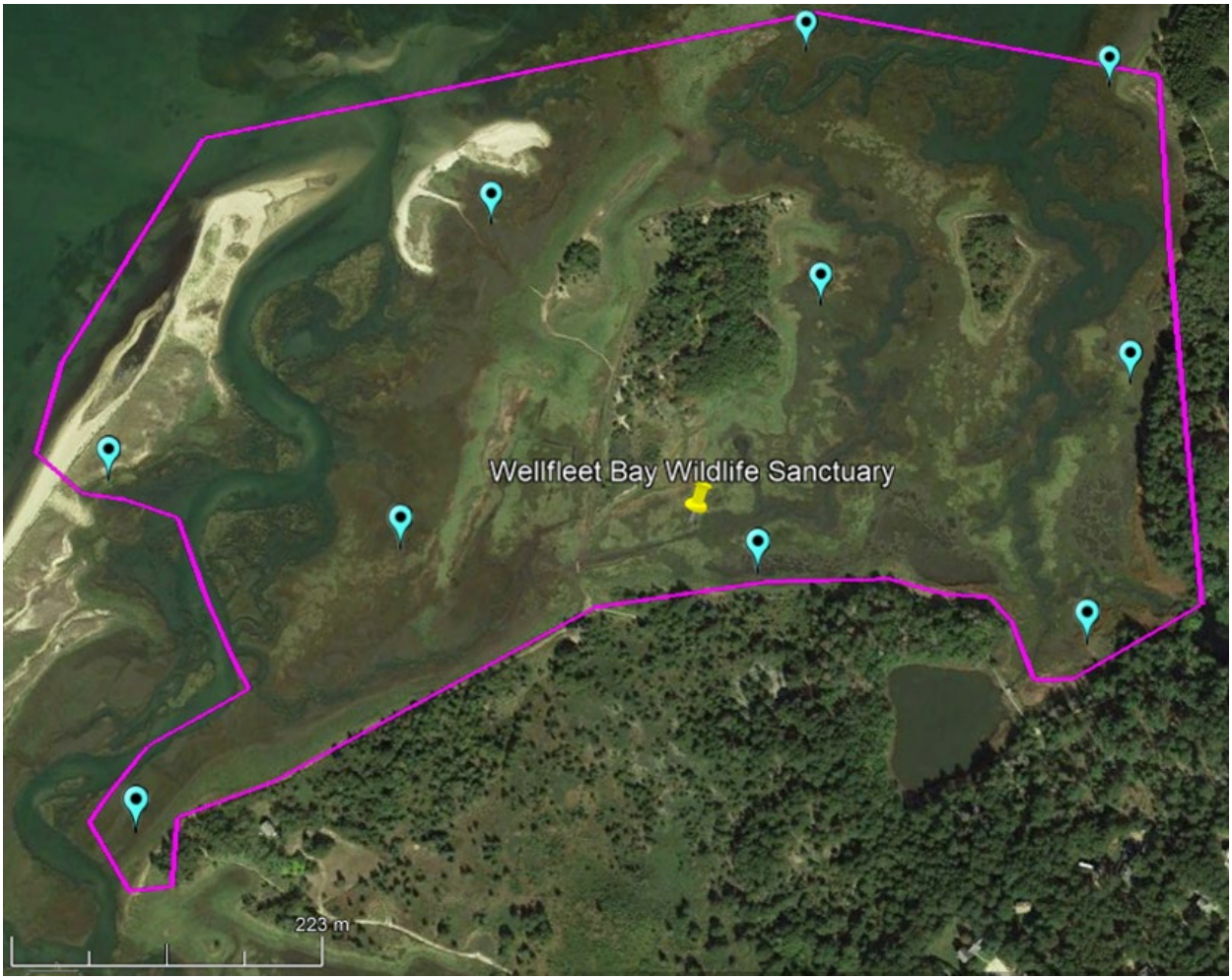

Figure 44 - Wellfleet Bay Wildlife Sanctuary (Wellfleet, MA) - Supported by the Massachusetts Audubon Society

Appendix B – Salt Marsh Classification

Minimum mapping unit (scale of the threats/vulnerability, phenomena)

Polygons: 2m x 2m, 4 sq m

Linear: 0.5 m x 3 m

First Level: Class (first digit - number)

1 - Vegetated: > 30% vegetation cover

2 - Water feature: 100% inundated at typical high tide with < 30% vegetation cover

3 - Bare ground: Exposed at typical high tide with < 30% vegetation cover

Second Level: Subclass (second and third digits - numbers)

1 - Vegetated: > 30% vegetation cover

01 - Low marsh (tall form *Spartina alterniflora* dominant): > 70%plant cover in tall form *S. alterniflora*

02 - Intermediate marsh (mix of high marsh vegetation and tall form *S. alterniflora*): high marsh species dominant with 5-40% tall form S. *alterniflora*

03 - Transitional marsh 1: short form *S. alterniflora* dominant (> 80%) mixed with typical high marsh species

04 - Transitional marsh 2: short form *S. alterniflora* common or dominant (30-80%) mixed with typical high marsh species

05 - Transitional marsh 3: *S. patens* & *D. spicata* dominant but mixed with 5-30% short form S. alterniflora

06 - High marsh 1: > 90% plant cover in *S. patens* & *D. spicata* and < 5% short form *S. alterniflora*

07 - High marsh 2: < 90% plant cover in *S. patens* & *D. spicata*, mixed with other high marsh species but < 10% shrub species and < 5% short form *S. alterniflora*

08 - *Juncus gerardii* band: > 50% of marsh vegetation is *Juncus gerardii*

09 - Salt-shrub marsh (high marsh vegetation mixed with shrub species): *S. patens* & *D. spicata* mixed with > 10% *Iva frutescens*, *Limonium carolinianum, Baccharis Halimifolia*

10 - *Salicornia* or *Suaeda* marsh: > 30% areal coverage and > 50% vegetative cover of *Salicornia spp.* and/or *Suaeda spp.*

11 - Brackish marsh: 50% of vegetative cover of brackish marsh species (e.g. *Schoenoplectus spp.*, *Bolboschoenus spp.*, *Typha spp.*)

12 - Brackish marsh - Phragmites: > 30% vegetative cover of *Phragmites australis*

13 - Vegetated ditch edges: mix of high marsh vegetation and intermediate form (neither tall nor short) Spartina alterniflora as linear features along the edges of water features (typically along the crown of ditch banks)

14 – High marsh vegetation mixed with a flowering white clover species

15 – Macroalgae fixed to the substrate of a shallow water feature

2 - Water: 100% inundated at typical high tide with < 30% vegetation cover

21 - Ditch: linear feature, straight lines often in a grid formation

22 - Natural creek: linear feature, branching and meandering

23 - Dug runnel: linear feature, ditch-like, but shallower (6” - 12”)

24 - Excavated sinuous creek: linear feature, like a natural creek but excavated, not natural

25 - Panne/pool: polygon feature, not associated with ditches or evidence of excavation (spoil piles)

26 - Artificial pool: polygon feature, associated with ditches or with evidence of excavation or berms/dikes

27 - Unvegetated bank: sloped topography on low marsh substrate in regularly flooded, intertidal zone

3 - Bare ground: exposed at typical high tide with < 30% vegetation cover

31 - High marsh substrate - deposition: < 30% living vegetation due to the presence of overwash or ice rafted soil deposition on high marsh substrate in an irregularly flooded zone

32 - High marsh substrate - wrack: < 30% living vegetation due to the presence of wrack/debris accumulation on high marsh substrate in an irregularly flooded zone

33 - High marsh substrate - dieback/denuded: bare ground on high marsh substrate in irregularly flooded zone

Third Level: Attributes (fourth digit - letter)

a. Healthy vegetation: < 30% of vegetation shows any indication of stress (discoloration, unusually stunted growth, thinning, foliage damage, wilting)
b. Stressed vegetation: > 30% of vegetation shows any indication of stress (discoloration, unusually stunted growth, thinning, foliage damage, wilting)
c. Cropped vegetation: > 30% of vegetation affected by herbivory
d. Algal mat: > 50% of surface covered with matted algae
e. Perforated peat: > 25 crab burrows per square meter
f. Low density peat: marsh peats demonstrates significantly less resistance to probing than healthy peat (greater amount of peat volume is air or water)
g. Slumping/eroding: > 50% of the area show indications of erosion or slumping
h. Hypersaline: indicators of hypersalinity, based on vegetation and salt deposits, are present
i. Artificially elevated: substrate, whether vegetated or not, has been anthropogenically elevated by the deposition of spoil or other material forming linear berms within the salt marsh
j. Water at low tide: water feature holds water throughout a typical tide cycle
k. Dewatered at low tide: water feature does not hold water at low tide during a typical tide cycle
l. Tidal flat: flat topography located in regularly flooded, intertidal zone
m. Maintained: artificial water feature (ditch, runnel, excavated sinuous creek, artificial pool) has been recently constructed or maintained
n. Non Maintained: artificial water feature (ditch, runnel, excavated sinuous creek, artificial pool) has does not appear to have been recently constructed or maintained
o. Excavated pool: artificial pool was created by excavation
p. Impounded pool: artificial pool was created by impoundment (including ditch plugs)
q. OMWM: water feature is part of an Open Marsh Water Management system
r. Widening: Water feature appears to be widening
s. Sediment deposit: naturally deposited sediment that reduces the aerial coverage of vegetation, either temporarily or permanently, by >20%
t. trash/debris washed onto the marsh that reduces the aerial coverage of vegetation, either temporarily or permanently, by >20%

Table of Attributes and Classes

Attribute	Vegetated	Water feature	Bare soil
a. Healthy vegetation	X	X	
b. Stressed vegetation	X	X	
c. Cropped vegetation	X	X	X
d. Algal mat		X	X
e. Perforated peat	X	X	X
f. Low density peat	X	X	X
g. Slumping/eroding	X	X	X
h. Hypersaline	X	X	X
i. Artificially elevated	X	X	X
j. Water at low tide		X	
k. Dewatered at low tide		X	
l. Tidal flat		X	
m. Maintained		X	
n. Unmaintained		X	
o. Excavated pool		X	
p. Impounded pool		X	
q. OMWM		X	
r. Widening		X	
s. Sediment deposit	X	X	X
t. Trash/Debris	X	X	X